Intra-grain Sr Isotope Evidence for Crystal Recycling and Multiple Magma Reservoirs in the Recent Activity of Stromboli Volcano,

JOURNAL OF PETROLOGY | VOLUME 46 | NUMBER 10 | PAGES 1997–2021 | 2005 | doi:10.1093/petrology/egi045

Intra-Grain Sr Isotope Evidence for Crystal Recycling and Multiple Magma Reservoirs in the Recent Activity of Stromboli Volcano, Southern Italy

LORELLA FRANCALANCI[1,2]*, GARETH R. DAVIES[3], WIM LUSTENHOUWER[3], SIMONE TOMMASINI[1,2], PAUL R. D. MASON[4] AND SANDRO CONTICELLI[1,2]

[1]DIPARTIMENTO DI SCIENZE DELLA TERRA, UNIVERSITÀ DEGLI STUDI DI FIRENZE, VIA LA PIRA 4, I-50121, FLORENCE, ITALY

[2]ISTITUTO DI GEOSCIENZE E GEORISORSE, CNR, SEZIONE DI FIRENZE, VIA LA PIRA, 4, I-50121, FLORENCE, ITALY

[3]DEPARTMENT OF EARTH AND LIFE SCIENCES, VRIJE UNIVERSITEIT, DE BOELELAAN 1085, 1081 HV AMSTERDAM, NETHERLANDS

[4]DEPARTMENT OF EARTH SCIENCES, UTRECHT UNIVERSITY, BUDAPESTLAAN 4, 3584 CD UTRECHT, NETHERLANDS

RECEIVED JUNE 2, 2004; ACCEPTED MARCH 30, 2005
ADVANCE ACCESS PUBLICATION JUNE 13, 2005

Over the last several hundred years, Stromboli has been characterized by steady-state Strombolian activity. The volcanic products are dominated by degassed and highly porphyritic (HP-magma) black scoria bombs, lapilli and lava flows of basaltic shoshonitic composition. Periodically (about one to three events per year), more energetic explosive eruptions also eject light coloured volatile-rich pumices with low phenocryst content (LP-magma) that have more mafic compositions than the HP-magma. An in situ *major and trace element and Sr isotope microanalysis study is presented on four samples chosen to characterize the different modes of activity at Stromboli: a lava flow (1985–1986 effusive event), a scoria bomb from the 'normal' present-day activity of Stromboli (April 1984), and a scoria and coeval pumice sample from a recent more explosive eruption (September 1996). Plagioclase ($An_{62–90}$) and clinopyroxene (Mg-number between 0·69 and 0·91) phenocrysts in all samples record marked major element variations. Large and comparable Sr isotope variations have been detected in plagioclase and clinopyroxene. HP-magma crystals have resorbed cores, with either high $^{87}Sr/^{86}Sr$ (0·70635–0·70630) or low $^{87}Sr/^{86}Sr$ (0·70614–0·70608); the latter values are similar to the values of the outer cores. Mineral rims and glassy groundmasses generally have intermediate $^{87}Sr/^{86}Sr$ (0·70628–0·70613). Similarly, mineral growth zones with three groups of $^{87}Sr/^{86}Sr$ values characterize minerals from the LP-pumice, with the lowest values present in mineral rims and groundmass glass. These results define a mixing process between HP- and LP-magmas, plus crystallization of clinopyroxene, plagioclase and olivine, occurring in a shallow magma reservoir that feeds the present-day magmatic activity of Stromboli. An important observation is the presence of a third component (high $^{87}Sr/^{86}Sr$ in mineral cores) considered to represent a pre-AD 1900 cumulus crystal mush reservoir situated just below the shallow magma chamber. These cumulus phases are incorporated by the LP-magma arriving from depth and transported into the shallow reservoir. A rapid decrease of $^{87}Sr/^{86}Sr$ in the replenishing LP-magma immediately prior to eruption of the AD 1985 lava flow is associated with an increased volume of LP-magma in the shallow magma chamber. The HP-magma in the shallow reservoir is not fully degassed when it interacts with the LP-magma, making efficient mixing possible that ultimately produces a well overturned homogeneous magma. Further degassing and crystallization occur at shallower levels as the HP-magma moves through a conduit to the surface.*

KEY WORDS: *isotopic microsampling; mineral recycling; mixing; Sr isotope disequilibria; Stromboli*

*Corresponding author. Telephone: +39 055 2757502. Fax: +39 055 2756242. E-mail: lorella.francalanci@unifi.it

INTRODUCTION

The last 1800 years of volcanic activity at Stromboli has consisted predominantly of mild explosions, at intervals of three to five per hour, which eject black scoria bombs, lapilli and ash of shoshonitic to high-K basaltic composition. This typical 'Strombolian' activity is sometimes interrupted by lava flows and more violent explosions that produce small volumes of light coloured pumice that represent up to 10% of the magma erupted. Although several recent papers have documented the behaviour of the present-day volcanic system of Stromboli (e.g. Giberti *et al.*, 1992; Allard *et al.*, 1994, 2000; Harris & Stevenson, 1997; Francalanci *et al.*, 1999, 2004; Métrich *et al.*, 2001; Bertagnini *et al.*, 2003), the detailed workings of this volcanic system remain poorly resolved. In particular, little is known of the processes that control the change from the typical moderately violent activity to the more vigorous explosions.

The petrographic, mineralogical and chemical characteristics of the magmas erupted during the last century record very minor variations, e.g. 2–2·5 wt % for K_2O and 30–50 ppm for Ni (Francalanci *et al.*, 2004). In contrast, starting in AD 1980–1985, Sr isotope ratios record a significant decrease (from 0·70626 to 0·70616). In addition, light coloured pumices have lower Sr isotope ratios than scoria and lavas (0·70610 and 0·70616, respectively; Francalanci *et al.*, 1999). These observations indicate that Sr isotope ratios may be useful in understanding the detailed magmatic behaviour of the present-day Stromboli volcano.

Isotope compositions have been successfully used to quantify magmatic processes such as crustal contamination and magma mixing, as they allow us to recognize the involvement of different components or sources. Isotope studies, however, have been applied generally to whole-rocks, despite the fact that bulk-rock compositions often represent a mechanical mixture of various phases with potentially different petrogenesis. Indeed, mineral–liquid elemental and isotopic disequilibria occur in many volcanic systems and are often key factors in revealing pre-eruptive magmatic processes (e.g. Feldstein *et al.*, 1994; Singer *et al.*, 1995; Davidson & Tepley, 1997; Wolff *et al.*, 1999; Ramos *et al.*, 2004). Mineral phases retain a history of changing conditions during their growth and, therefore, usually record magma differentiation processes in more detail than the whole-rock. In order to provide the spatial resolution needed to determine the temporal evolution recorded in a mineral within a volcanic rock, laser ablation (e.g. Davidson *et al.*, 2001; Ramos *et al.*, 2004) and microdrilling have been used on phenocryst minerals and associated glass (Davidson & Tepley, 1997; Davidson *et al.*, 1998; Knesel *et al.*, 1999; Tepley *et al.*, 1999, 2000; Perini *et al.*, 2003). The glass represents a proxy of the magma composition immediately prior to eruption.

This paper reports the results of a study of mineral–melt Sr isotope disequilibrium in samples from the activity of Stromboli at the end of the 20th century, obtained by the microdrilling method. These data, combined with *in situ* major and trace element data for the minerals, are used to improve our understanding of the pre-eruptive magmatic processes that control the style of the present-day Strombolian activity.

VOLCANIC AND MAGMATIC HISTORY

Stromboli Island is located on continental crust of 20 km thickness and is the northernmost stratovolcano of the Aeolian volcanic arc in the southern Tyrrhenian Sea (Fig. 1). The island rises from a depth of about 2000 m below sea level to an elevation of 924 m above sea level (Morelli *et al.*, 1975). The volcano has a total volume of $\sim$300 km^3. The oldest subaerial rocks of the island formed about 100 kyr ago, whereas the Strombolicchio neck, located 1·7 km NE of Stromboli Island, and belonging to the same submarine edifice, is significantly older, with an age of 204 $\pm$ 25 ka (Gillot & Keller, 1993).

Six main periods of effusive and explosive activity characterize the magmatic history of the subaerial part of Stromboli. From oldest to the youngest, these periods are: Paleostromboli I, II, III, Vancori, Neostromboli and Recent (Fig. 1) (Francalanci *et al.*, 1993; Hornig-Kjarsgaard *et al.*, 1993; Pasquarè *et al.*, 1993). Eight edifice collapses of variable nature (crater, caldera, flank and sector) have alternated with periods of volcano building. The more recent sector collapses led to the formation of the Sciara del Fuoco depression on the NW flank of the volcano, where most of the products of the present-day activity are usually accumulated (Rosi, 1980; Pasquarè *et al.*, 1993; Kokelaar & Romagnoli, 1995; Tibaldi, 2001; Tibaldi *et al.*, 2003). During its entire history, Stromboli has produced magmas of highly variable composition, ranging from calc-alkaline (mainly basaltic andesites), to potassic-alkaline (potassic trachybasalts and shoshonites), through high-K calc-alkaline (high-K basalts and andesites) and shoshonitic (shoshonitic basalts to trachytes) types. The transition from one period of effusive and explosive activity to another is usually associated with major changes in magma composition (Francalanci *et al.*, 1988, 1989, 1993; Hornig-Kjarsgaard *et al.*, 1993). Calc-alkaline lava flows are from the Strombolicchio neck and Paleostromboli II period ($\sim$60 ka). Pyroclastic deposits and lavas erupted during the Paleostromboli I ($\sim$85 ka) and III ($\sim$35 ka) periods have mainly high-K calc-alkaline compositions.

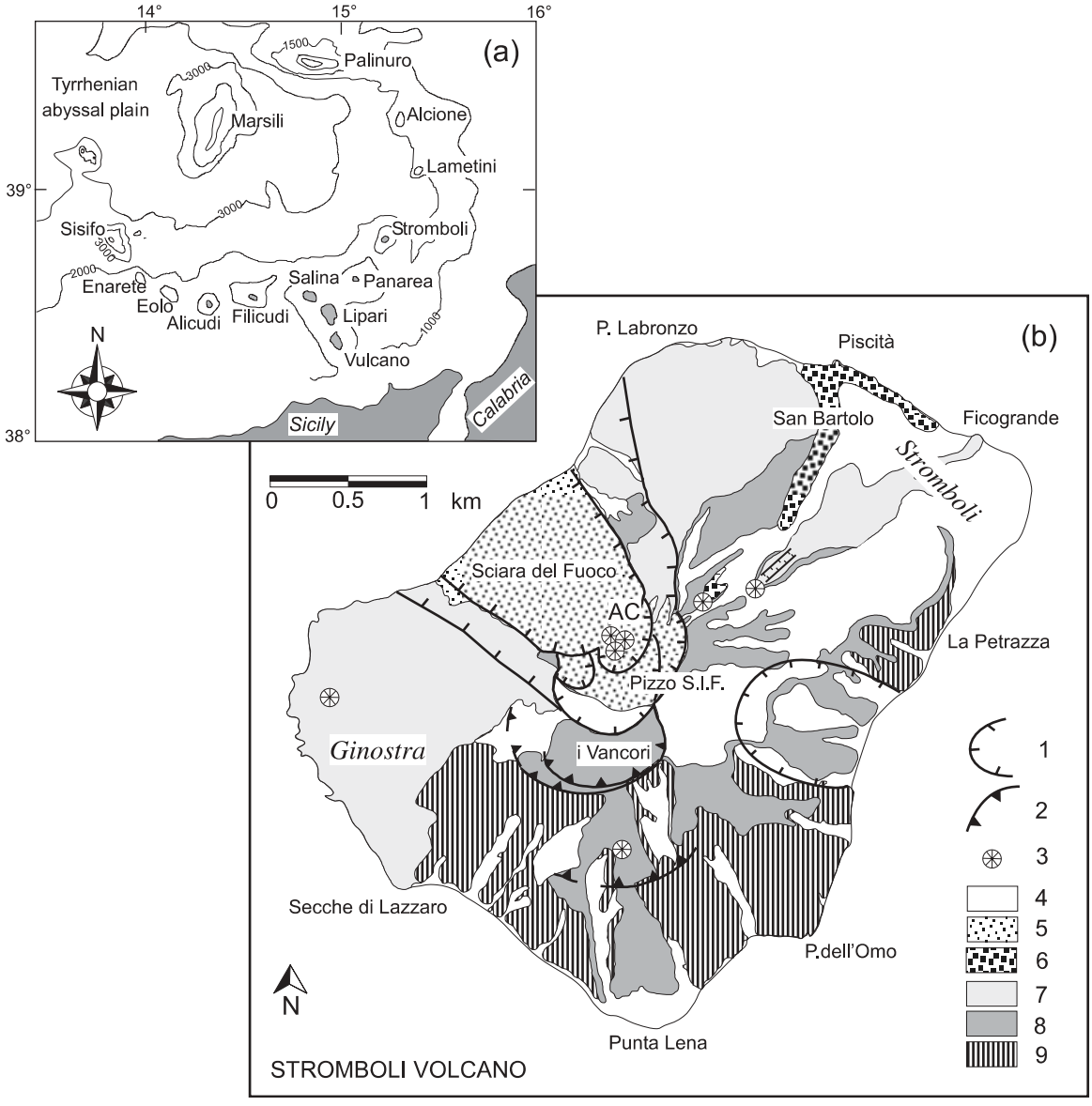

Fig. 1. (a) Stromboli location: bathymetric map of the Aeolian volcanic arc (southern Tyrrhenian Sea, Italy), formed by seven main islands (in grey) and several seamounts. (b) Simplified geological map of the Stromboli volcano. 1: sector collapses; 2: caldera collapses; 3: craters; 4: epiclastic deposits; 5: Recent and present-day periods (younger than ~5 ka; high-K calc-alkaline and shoshonitic basalts); 6: lavas of San Bartolo unit (Recent period, ~2 ka; high-K calc-alkaline basalts); 7: Neostromboli period (~13–5 ka; potassic series); 8: Vancori period (26–13 ka; shoshonitic series); 9: Paleostromboli I, II and III (~100–35 ka; calc-alkaline, high-K calc-alkaline and shoshonitic series). AC, Active craters; Pizzo S.l.F., Pizzo Sopra la Fossa. Modified after Keller *et al.* (1993) and Tibaldi (2001).

The activity of the Vancori period (~26–13 ka) was mostly characterized by shoshonitic lava flows that at present form one (924 m above sea level) of the two peaks of the island (Fig. 1). Thin lava flows with basic potassic-alkaline composition were erupted during the Neostromboli period (~13–5 ka) from central and eccentric vents. Effusive and Strombolian activity, erupting shoshonitic ('Pizzo Sopra la Fossa' and present-day rocks) and high-K basalts ('San Bartolo lavas') mainly characterize the Recent period of activity (younger than ~5 ka). The pyroclastic cone of Pizzo Sopra la Fossa, which forms the second peak of the volcano (918 m above sea level), represents the first eruptive event of the Recent period (Francalanci *et al.*, 1989, 1993; Gillot & Keller, 1993; Hornig-Kjarsgaard *et al.*, 1993;).

The change in magma composition from calc-alkaline to potassic lavas is associated with a general increase in incompatible trace element contents. There is, however, no positive correlation of K_2O with Sr isotope ratios, despite individual calc-alkaline and

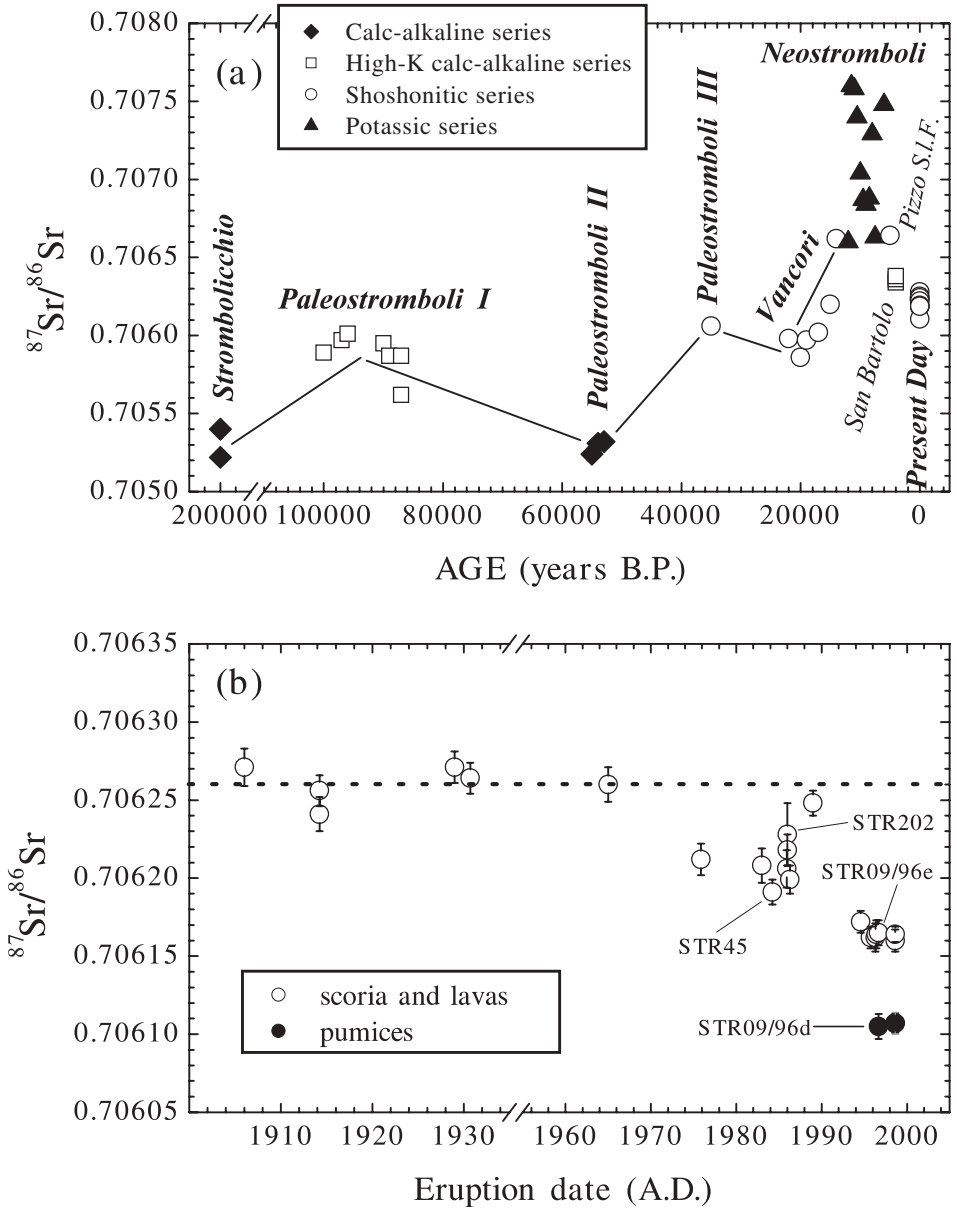

Fig. 2. Variation of Sr bulk-rock isotope ratios with time for the subaerial rocks of Stromboli. (a) From 200 ka to present-day period; symbols indicate the different magmatic series. Pizzo S.l.F., pyroclastic deposits of Pizzo Sopra la Fossa cone; San Bartolo, lavas of San Bartolo unit. (b) Twentieth century period; symbols indicate the sample lithologies. The names of the samples studied by microdrilling are also indicated. Data from Francalanci *et al.* (1988, 1989, 1999, 2004). As a result of the high error in the published Sr isotope composition of STR45 whole-rock (Francalanci *et al.*, 1988), $^{87}Sr/^{86}Sr$ was re-analysed in this sample, resulting in a lower isotope ratio and error.

potassic-alkaline magmas having the most extreme $^{87}Sr/^{86}Sr$ values (0·70519–0·70538 and 0·70660–0·70757, respectively; Francalanci *et al.*, 1988; Luais, 1988) (Fig. 2a). Shoshonitic and high-K calc-alkaline rocks from Paleostromboli I, Paleostromboli III and the Vancori period, for example, have similar Sr isotope ratios (0·70583–0·70603), and these isotope ratios are lower and less variable than those of the shoshonitic and high-K calc-alkaline products from the Recent period (0·70608–0·70660; Fig. 2) (Francalanci *et al.*, 1988, 1989, 1993, 1999, 2004).

CHARACTERISTICS OF THE PRESENT-DAY VOLCANIC ACTIVITY

The present-day activity occurs from four vents, situated at 750 m above sea level inside the Sciara del Fuoco depression and below the Pizzo Sopra la Fossa peak

(Fig. 1). The 'normal' mildly explosive activity ejects blocks, black scoria bombs, lapilli and ash to variable heights (from a few tens to hundreds of metres) at intervals of about three to five events per hour. The ejecta usually fall around the craters and accumulate at the base of the Sciara del Fuoco scar. The volcanic activity is generally accompanied by a continuous stream of gas, which is mainly composed of H_2O, CO_2 and SO_2 (Allard *et al.*, 1994, 2000).

At variable time intervals (*c.* 4 years, on average), the normal moderately explosive activity is punctuated by lavas flowing into the Sciara del Fuoco depression. Lava production lasts from <3 days to 11 months (Capaldi *et al.*, 1978; Barberi *et al.*, 1993). Recent notable effusive events occurred from December 1985 to April 1986 (De Fino *et al.*, 1988) and a conspicuous lava flow eruption started on 28 December 2002 and ended on 20 July 2003.

More violent explosions than normal occur with a frequency of about one to three events per year (Barberi *et al.*, 1993; Bertagnini *et al.*, 1999). During these eruptions, referred to as 'major explosions', metre-sized scoriaceous bombs and blocks are ejected several hundreds of metres, reaching the Pizzo Sopra la Fossa peak and the upper path to the craters. Lapilli and ash can reach the coastal zones. Only rarely have coarse blocks and bombs reached the coast around the island, causing injury to the inhabitants and/or damaging property. These most violent eruptions are referred to as 'paroxysms', a good example of which was the 1930 eruption (Barberi *et al.*, 1993). A paroxysmal explosion also occurred on 5 April 2003, when the lava flow was still active. Tsunamis have been produced during paroxysm crises and by landslides along the Sciara del Fuoco scar. The best-documented tsunami occurred on 30 December 2002, which was triggered by a landslide phenomenon connected with the lava flow eruption (Bonaccorso *et al.*, 2003).

The normal mildly explosive activity usually erupts a volatile-poor, highly porphyritic magma (hereafter, the 'HP-magma'), forming black scoria, scoriaceous bombs and lapilli. The lava flows are of similar composition. In contrast, two types of magmas are usually emitted during major explosions and paroxysms. During the more energetic eruptions, the most voluminous juvenile component (~90%) consists of black scoria similar in composition to that produced by normal activity. The second component (~10%) consists of a highly vesiculated light pumice, representing a volatile-rich magma with low phenocryst content (hereafter, the 'LP-magma') (Bonaccorso *et al.*, 1996; Bertagnini *et al.*, 1999; Francalanci *et al.*, 1999, 2004; Métrich *et al.*, 2001). Black scoria and light pumice can be found mingled in a single hand specimen. The presence of two types of magma seems to be a fundamental feature of the current persistent Strombolian activity that began between the third and seventh centuries AD (Rosi *et al.*, 2000).

Petrography and mineralogy

Black scoria and lavas

Black scoria and lavas have highly porphyritic seriate textures (~45–60 vol. % of phenocrysts and microphenocrysts) with a glassy groundmass in the scoria, and microcrystalline or hypo-crystalline groundmass in the lavas. Plagioclase is the most abundant mineral phase (on average, ~35 vol. %), followed by clinopyroxene (on average, ~15 vol. %) and olivine (on average, ~5 vol. %). Microphenocrysts mostly comprise plagioclase and some olivine.

The largest phenocryst phase is clinopyroxene, which is sometimes >1 cm in length. The composition of clinopyroxene ranges from augite to diopside, with Mg-number [molar $Mg^{2+}/(Mg^{2+} + Fe^{2+})$] mainly between 0·70 and 0·91. This wide range of compositional variation has remained nearly the same for at least the last 100 years, and can be found in a single sample, and even in a single large crystal. The crystals of larger size are usually oscillatory zoned, with diopsidic or augitic cores, generally diopsidic outer cores and always augitic outer rims (e.g. Fig. 3). Cores are usually partially resorbed. The clinopyroxenes in equilibrium with the groundmass composition, represented by the rims of phenocrysts and the microphenocrysts, have Mg-number around 0·74–0·78.

Olivine is the second largest mineral phase, with crystals commonly around 0·1–0·2 cm. Olivine from black scoria and lavas is usually in equilibrium with the groundmass, and its composition has not significantly changed since the beginning of the 20th century, ranging from Fo_{64} to Fo_{74}, with an average of Fo_{70}. When present, zoning is weak, normal or reverse (2–3% variation in Fo; Francalanci *et al.*, 2004).

The plagioclase phenocryst population is dominated by grains less than 0·5 mm in length and the larger grains, of >0·5 cm, form less than 10 vol. %. The compositional range of plagioclase ($An_{60–87}$) has been nearly the same since the beginning of the 20th century. The entire compositional range can be found in a single hand specimen. The largest plagioclase crystals usually have resorbed cores and complex zoning in the rims, with sieve textures found either in the cores or in repeated growth layers (e.g. Fig. 4). Despite the presence of variable mineral zonation, the outer rims are usually An_{65} (e.g. Fig. 4), representing the composition of plagioclase in equilibrium with the groundmass composition (Francalanci *et al.*, 2004).

Glomeroporphyritic aggregates of olivine and clinopyroxene, with interstitial plagioclase, are common in the scoria and lava rock type.

Light pumice

Light pumice has a weakly porphyritic seriate texture (<10 vol. % phenocrysts, usually ~5 vol. %) with a glassy

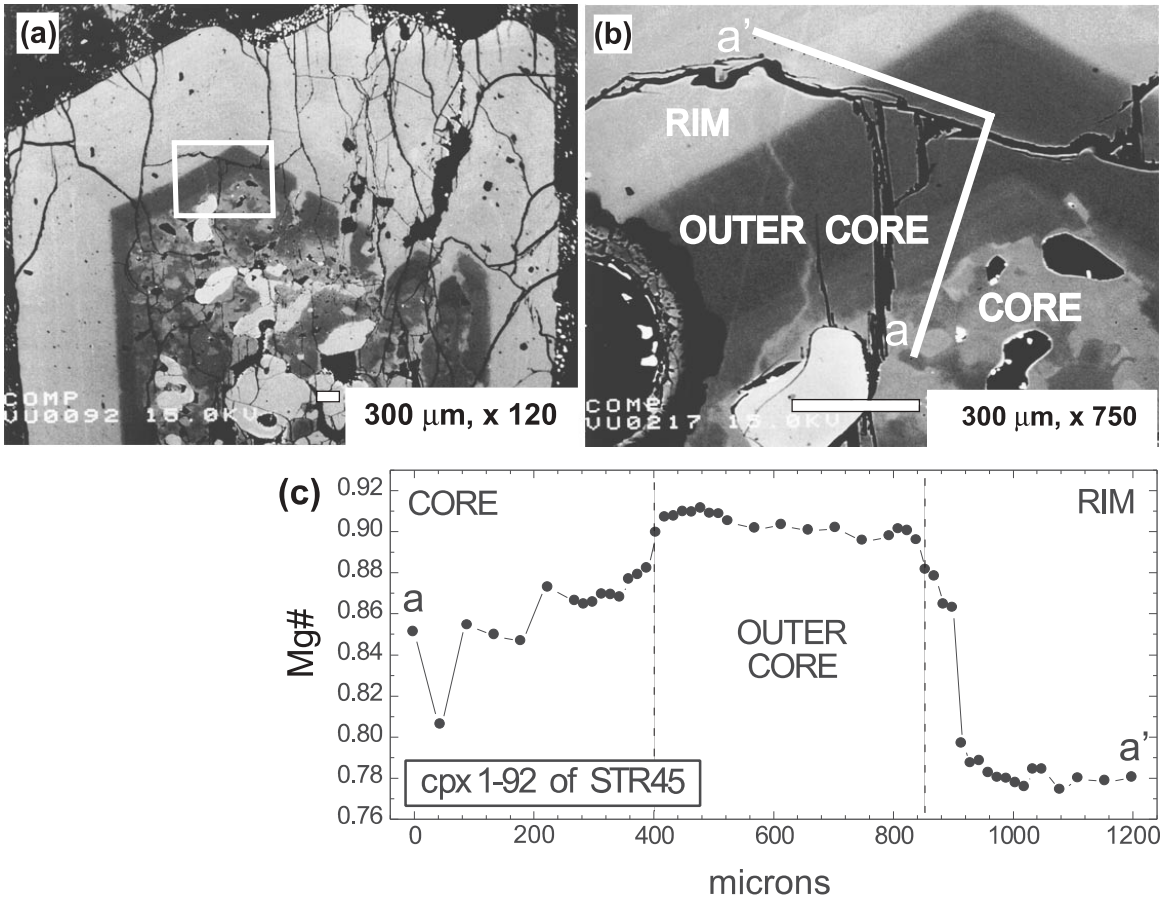

Fig. 3. Complex zoning, with resorbed core, in a representative clinopyroxene (cpx 1-92 of STR45). (a) and (b), Electron microprobe backscattered image: (b) is the enlarged view of the inset area in (a). Length of scale bar and magnification each are shown in each image. (c) Core–rim compositional variations analysed along the a–a′ profile shown in (b). Note that the profile does not represent the compositions of the entire core and rim.

groundmass. Phenocryst minerals consist of olivine, clinopyroxene and plagioclase, with variable proportions in different samples. Euhedral crystals are usually smaller than those of the black scoria and lavas (<0·5 mm), with a large prevalence of microphenocrysts. Petrographic and mineralogical evidence suggests that most of the largest minerals crystallized from the HP-magma (e.g. crystals in compositional equilibrium with, and often surrounded by, a more evolved glass than the pumice glassy groundmass) and were included into the LP-magma by syn-eruptive mingling processes (Francalanci *et al.*, 2004).

Olivine in the light pumice has a large compositional range ($Fo_{68–86}$). Nevertheless, the olivine in equilibrium with the groundmass composition has the highest forsterite composition ($Fo_{81–86}$), so that $(FeO/MgO)_{olivine}/(FeO/MgO)_{liquid}$ is between 0·35 and 0·25. The cores of some of the phenocrysts have compositions similar to those of olivine in scoria and lava, which contrasts with the higher Fo contents of the rims and microphenocrysts. Thus, phenocryst zoning is sometimes strong and reverse.

Clinopyroxenes from the pumice show the same compositional range as that found in the clinopyroxenes of the scoria and lavas, with Mg-number between 0·69 and 0·91. The clinopyroxene crystals in or close to equilibrium with the groundmass composition are those with Mg-number >0·83. Zoning of phenocrysts is oscillatory, but the outer rims usually have high Mg-number (0·84–0·91), similar to those of the microphenocrysts.

Despite the variable An content of the plagioclase ($An_{60–90}$), microphenocrysts and the rims of phenocrysts that are clearly formed from the LP-magma usually have An >80%. Individual phenocrysts display strong (e.g. $An_{65–85}$) and complex zoning, which can be reverse or oscillatory. Cores frequently are partially resorbed, and have variable An contents, with the outer rims usually having the highest An content. Microphenocrysts are also zoned, but the An variation is smaller (e.g. $An_{84–88}$) (Francalanci *et al.*, 2004).

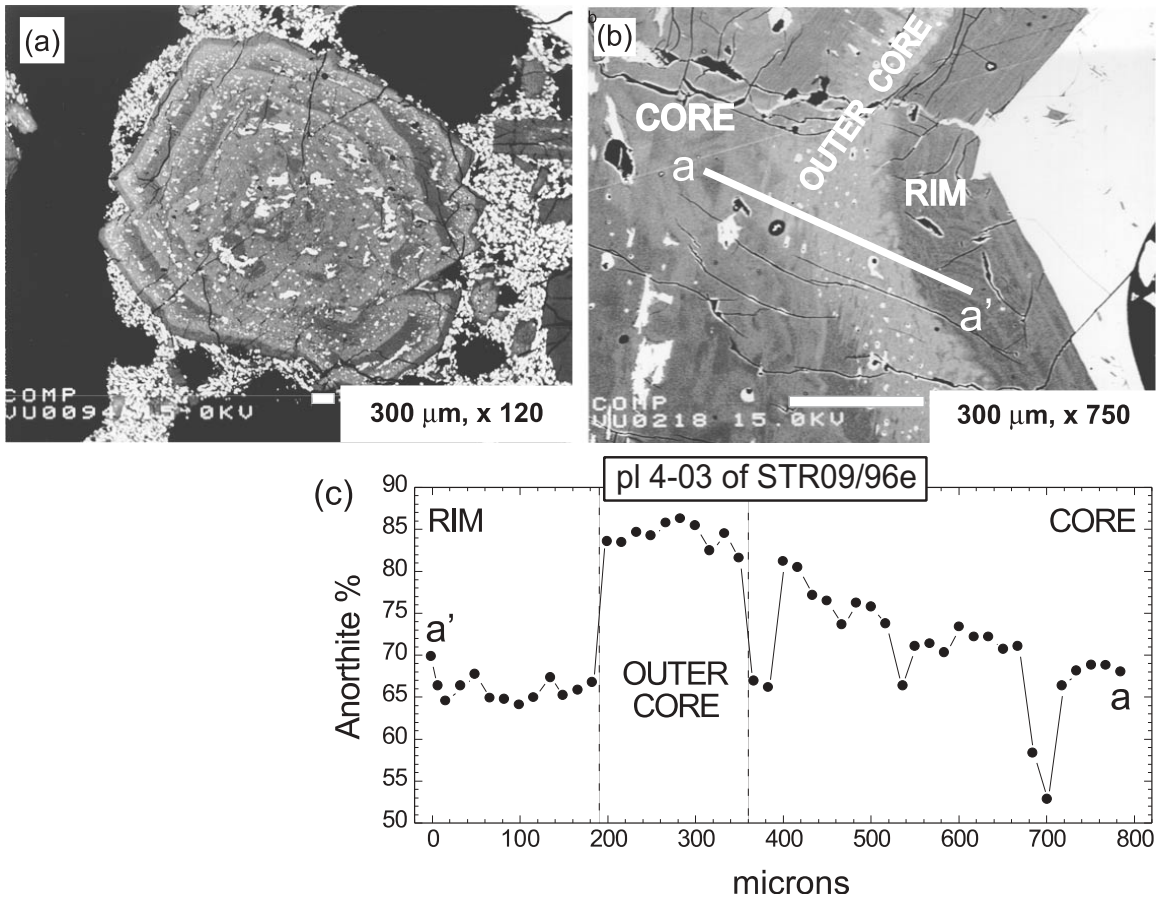

Fig. 4. Complex zoning in two representative plagioclases. (a) and (b) are electron microprobe back-scattered images. Length of scale bar and magnification are shown in each image. (c) Core–rim compositional variations analysed in the plagioclase pl 4-03 of STR09/96e along the a–a′ profile shown in (b). Note that the profile does not represent the compositions of the entire core and rim.

Geochemical composition of whole-rocks and glasses

Since the onset of the Strombolian activity, the rocks erupted have been high-K and shoshonitic basalts. The shoshonitic terminology derives from the classification of Peccerillo & Taylor (1976), and is well established in Stromboli literature. According to the TAS classification of Le Maitre (2002), however, the term potassic trachybasalts is preferred. To be consistent with previous publications on Stromboli, we retain the term shoshonitic basalt here. LP-magmas, erupted as pumices, are slightly less evolved than the HP-magmas, erupted as scoria and lavas, with lower silica and K_2O contents (SiO_2 48·2–49·2 wt % and 48·6–51·5 wt %, and K_2O 1·5–2 wt % and 2–2·5 wt %, respectively). HP-magmas have slightly higher incompatible trace element contents, except for Sr, and lower MgO, V, Ni, Co and Sc abundances than LP-magmas (Rosi *et al.*, 2000; Francalanci *et al.*, 2004, and references therein).

The compositions of pumice glasses (LP-magma type) are distinct from those of scoria and lava glasses (HP-magma type). Pumice glasses are shoshonitic basalts, whereas scoria and lava glasses have more evolved compositions, with SiO_2 and K_2O contents of 51–53 and 3·5–5·2 wt %, respectively. Scoria and lava glasses have lower MgO, CaO, Al_2O_3 and Sr, and higher P_2O_5, TiO_2, FeO, Na_2O and Ba content than the pumice glasses. Compositional gaps in MgO (between 3·8 and 5·5 wt %), CaO (7·8–10 wt %), Al_2O_3 (16–17 wt %) and FeO (8·6–9·2 wt %) are present between the pumice glasses and the scoria and lava glasses.

Sr isotope ratios of scoria and lavas (HP-magmas) from the beginning of the 20th century to around 1980 are constant, with an average of 0·70626 (±2, 2σ) (Fig. 2b). After 1980, $^{87}Sr/^{86}Sr$ smoothly decreases to a value of 0·70615 in the AD 2003 scoria (Francalanci *et al.*, 1999, 2004). Pumice samples (LP-magmas) from the AD 1996 and 1998 eruptions have significantly lower Sr isotope ratios than the scoria, with $^{87}Sr/^{86}Sr$ ~0·70610 (Fig. 2b). The decrease in Sr isotope ratios with time since around AD 1980 has been used to demonstrate the short residence time (≈19 years) of the magma feeding the

volcanic activity at Stromboli (Francalanci *et al.*, 1999). Nd isotope ratios of scoria, lavas and pumice from the AD 1996 and 1998 major eruptions are essentially constant (0·51256 ± 1; Francalanci *et al.*, 2004).

ANALYTICAL TECHNIQUES

Four samples were selected for Sr isotope analysis in order to investigate different time periods and styles of eruptions during the last century (Fig. 2b). Two rocks representative of HP-magmas were selected from the time period when Sr isotope ratios started to decrease: black scoria (STR45) erupted during normal, moderately explosive activity on 28 April 1984, and a sample of the 1985–1986 lava flow (STR202), taken on 13 December 1985 at the sea delta formed at the base of Sciara del Fuoco. The other two samples studied represent HP- and LP-magmas ejected during the same major eruption on 4 September 1996, when Sr isotope ratios had already decreased significantly: these are a black scoria (STR09/96e) and a pumice (STR09/96d) sample, respectively.

Doubly polished, thin sections, each of 1250 micron thickness, were prepared for microdrilling. Prior to drilling, back-scattered electron (BSE) images were obtained, and mineral compositions analysed by electron microprobe, on a total of 40 clinopyroxene and plagioclase grains, in order to check the extent of major element zonation. All the grains studied were zoned; microdrilling was, therefore, performed on grains showing typical and the most extreme major element variation. Mineral grains were studied optically, and only grains with growth zones approximately perpendicular to the polished surface were selected for further study, i.e. ensuring that drilling would stay approximately in the same growth band. *In situ* analyses of trace elements by laser ablation ICP–MS were also performed prior to drilling of selected crystals.

The microdrilling was performed using a Merchantek computer-controlled drilling system, using diamond impregnated drill tips (~50 microns diameter). A 200 micron wide and ~1000 micron deep hole was excavated around the entire mineral, making sure that all glass and groundmass was separated from the host grain. This usually caused the loss of 5–10 microns of the outer rim of the grain. Thick sections were then cleaned in an ultrasonic bath to remove all the powder. Concentric zones of the mineral could then be drilled with a resolution of better than 5 microns. Cleaning was required between sampling of each growth band. Sampling depths varied from 350 to 750 microns, whereas sampling width ranged from 50 microns (usually in the rims) up to 4–5 mm (in some cores). Sampling volumes were designed to ensure that measured Sr isotope ratios were not compromised by a significant blank contribution (Table 1).

Sr isotope ratios were determined at the Vrije Universiteit using standard chemical separation techniques (SrSpec Resin©) and a Finnigan 262 RPQ-plus© Thermal Ionization Mass Spectrometer equipped with eight Faraday collectors. $^{87}Sr/^{86}Sr$ values were measured dynamically in a triple jump routine and corrected using an exponential mass fractionation law to $^{86}Sr/^{88}Sr = 0{\cdot}1194$. During this project, replicate measurement of NBS 987 gave mean values of $^{87}Sr/^{86}Sr = 0{\cdot}710247 \pm 11$ (2 SD, $n = 18$). Five total Sr blanks were measured during the course of this study, yielding 66·3 ± 4·8 pg, with an average $^{87}Sr/^{86}Sr$ of 0·70989 ± 9. The blank $^{87}Sr/^{86}Sr$ ratios were determined in static mode. Sr concentrations of drilled samples are not known precisely but were estimated from sample volumes (Table 1) and from the Sr contents of minerals analysed. The maximum estimated blank contribution is in the order of 0·1% and, in most cases, significantly less than 0·01%. Therefore, no blank corrections have been made to the measured Sr isotope ratios.

Quantitative wavelength-dispersive electron microprobe analyses were performed using a JEOL JXA-8800M at an excitation voltage of 15 kV and a beam current of 25 nA, with counting times of 25 s (major elements) to 50 s (trace elements). The following standards were used for analysis of clinopyroxene, olivine and plagioclase: F: fluorite; Na: jadeite; Mg: diopside (olivine for olivines); Al: gehlenite (synth. Al_2O_3 for plagioclase scans); Si: diopside (olivine for olivines); P: apatite; S: anhydrite; Cl: marialite; K: orthoclase; Ca: diopside; Ti: synth. $FeTiO_3$; Cr: synth. Cr_2O_3; Mn: synth. Mn_2SiO_4; Fe: olivine (fayalite for clinopyroxene scans); Ni: synth. NiO; Sr: celestine. For major elements in glass (Mg, Al, Si, Ca and Fe), a MORB-glass standard was used (JDF-D2#2 of Lamont–Doherty Earth Observatory, Columbia University, USA). Clinopyroxene and olivine were measured with a focused electron beam. In order to minimize damage by the electron beam, plagioclase and glass were measured using a defocused spot of 10 μm, or, for very small grains or zones, 3–5 μm. Data were ZAF-corrected using the online JEOL correction program. Major-element standards were routinely included as unknowns to validate the analytical procedure.

Laser ablation ICP–MS analyses were performed at Utrecht University using a 193 nm GeoLas 200Q laser ablation system and a Micromass Platform quadrupole ICP–MS system (described in detail by Mason & Kraan (2002). Ablation was performed at a fixed point on the sample with a laser fluence of 15 J/cm^2, giving ablation craters of 120 μm in diameter and <100 μm deep. Concentrations were calculated using NIST SRM 612 as a calibration standard (Pearce *et al.*, 1997) with ^{44}Ca as an internal standard isotope using Ca data previously determined by electron microprobe analysis. Data reduction protocols, following time and depth resolved

Table 1: Sr isotope ratios in microdrilled portions of analysed clinopyroxene (cpx) and plagioclase (pl) with ranges of anorthite (An) content (%) for pl and Mg-number [molar $Mg^{2+}/(Mg^{2+} + Fe^{2+})$] for cpx

Sample	Grain	Sample type	$^{87}Sr/^{86}Sr$	$2\sigma_m$	B × L × D (mm)	An or Mg-no.	ICP–MS
STR45		*Highly porphyritic scoria*					
28/04/84		whole-rock	0·706191	8			
		glassy groundmass	0·706269	8			
	pl 3–92	resorbed core	0·706345	12	0·5 × 0·4 × 0·35	59·2	
		outer core (mi)	0·706175	10	0·1 × 5·2 × 0·75	76·5	
		rim	0·706295	10	0·3 × 6·2 × 0·25	62·5–64·4	
	pl 6–91	resorbed core	0·706343	10	0·8 × 0·2 × 0·75	71·1–74·5	
		outer core	0·706163	9	0·035 × 4 × 0·5	79·9	
		inner rim	0·706265	12	0·1 × 5 × 0·35	63·5–65·1	ICP–MS
		outer rim	0·706289	11	0·08 × 7 × 0·25	63·8–66·8	ICP–MS
	pl 7–91	core (mi)	0·706171	9	0·6 × 0·5 × 0·5	76·5–78·3	
		rim	0·706287	11	0·1 × 3·5 × 0·45	65·0–66·8	
	pl 9–91	outer rim	0·706291	12	0·08 × 5 × 0·35	58·5–65·3	
		outer core at 150 μm	0·706182	12	0·05 × 3·5 × 0·35	78·8–79·0	
		resorbed core (mi)	0·706346	11	0·1 × 0·6 × 0·5	64·7–65·2	
	cpx 1–92	outer rim	0·706272	10	0·1 × 7·5 × 0·5	0·76	ICP–MS
		inner rim (i) at 150 μm	0·706281	9	0·125 × 7 × 0·5	0·78	
		inner rim (ii) at 250 μm	0·706284	9	0·15 × 6·5 × 0·6		
		outer core	0·706154	8	0·1 × 4·5 × 0·75	0·90	ICP–MS
		core (ol + mi)	0·706335	8	0·5 × 1 × 0·75	0·79–0·90	
		core (mi)	0·706177	10	0·5 × 0·5 × 0·75		ICP–MS
	cpx 3–91	core	0·706289	10	0·5 × 0·5 × 0·75	0·75–0·78	ICP–MS
		rim	0·706283	9	0·3 × 4 × 0·35	0·76–0·78	ICP–MS
	cpx 4–91	core	0·706142	10	1 × 0·3 × 0·75	0·88–0·91	
		inner rim at 0·5 mm	0·706279	10	0·1 × 4·5 × 0·5	0·77–0·78	
		outer rim	0·706282	8	0·1 × 5·8 × 0·5	0·75	
	cpx 5–91	core	0·706325	10	0·6 × 0·35 × 0·75	0·72–0·75	ICP–MS
		outer core	0·706185	10	0·2 × 4·2 × 0·5	0·83–0·85	ICP–MS
		outer rim	0·706285	8	0·15 × 5·1 × 0·5	0·76	ICP–MS
STR202		*Highly porphyritic lava*					
13/12/85		whole-rock	0·706228	20			
		glassy groundmass	0·706166	8			
	pl 1–202	core	0·706261	10	0·65 × 0·75 × 0·75		
		rim	0·706163	11	0·15 × 5·3 × 0·25		
	pl 2–202	core	0·706257	11	0·45 × 1·25 × 0·75		
		rim	0·706167	12	0·15 × 4·9 × 0·25		
	cpx 1–202	core	0·706253	12	0·85 × 1·5 × 0·75		
STR09/96d		*Low porphyritic pumice*					
04/09/96		whole-rock	0·706105	8			
		glassy groundmass	0·706094	9			
		plagioclase total	0·706115	12	0·4 × 2 × 0·75		
	pl 1–01	outermost rim	0·706085	12	0·25 × 4·5 × 0·35	88·1	
	pl 1–01	core (mi)	0·706276	12	0·8 × 1·5 × 0·25	65·3–75·4	
	pl 1–02	inner rim (mi)	0·706092	10	0·25 × 4·9 × 0·2		
	pl 1–02	core	0·706125	11	0·7 × 1·8 × 0·3	80·7	
	pl 2–02	rim (mi)	0·706082	10	0·2 × 6·5 × 0·2	81·0–85·1	
	pl 2–02	core	0·706151	11	0·6 × 2 × 0·5	88·5–89·5	
	pl 4–00	rim	0·706098	12	0·075 × 5·5 × 0·35	88·1	
	pl 8–00	core (mi)	0·706183	12	0·55 × 1·5 × 0·35	75·3–83·7	
	pl 8–00	outer core	0·706257	12	0·1 × 8·5 × 0·5	65·3–67·8	
	pl 8–00	inner rim	0·706157	9	0·08 × 6·5 × 0·5	79·9	
	pl 3–02	rim	0·706103	11	0·075 × 6·5 × 0·45	89·5	
	pl 3–02	core (mi)	0·706161	10	0·5 × 2·5 × 0·5	79·2–83·6	
	cpx 1–02	core	0·706147	11	2·5 × 3·5 × 0·75	0·73–0·75	
		rim	0·706103	10	0·1 × 3·85 × 0·75	0·84	

Table 1: continued

Sample	Grain	Sample type	$^{87}Sr/^{86}Sr$	$2\sigma_m$	B × L × D (mm)	An or Mg-no.	ICP–MS
STR09/96e		*Highly Porphyritic scoria*					
04/09/96		whole-rock	0·706165	8			
	cpx 1–03	core (mi)	0·706331	9	4·5 × 2·4 × 0·75	0·74–0·77	ICP–MS
		core	0·706054	10	2·1 × 2·5 × 0·75	0·89	
		inner rim	0·706116	8	0·5 × 1·5 × 0·75	0·76	ICP–MS
		outer rim	0·706124	9	0·25 × 3·4 × 0·5	0·74–0·75	ICP–MS
	cpx 2–03	resorbed core (ol)	0·706317	10	4 × 1·6 × 0·75	0·70–0·72	
		outer core	0·706098	9	4·5 × 1·5 × 0·75	0·77–0·81	
		banded rim	0·706147	8	1·5 × 2·5 × 0·5	0·74–0·76	
	pl 4–03	core (mi)	0·706325	11	4 × 4 × 0·75	68·8–85·5	
		outer core (mi)	0·706105	10	0·15 × 2·5 × 0·5	84·0–86·1	
		rim	0·706125	12	0·1 × 4·5 × 0·25	63·4–70·2	
	pl 5–04	core (mi)	0·706082	10	0·5 × 4 × 0·75	74·8–82·1	
		inner rim	0·706129	9	2 × 2·2 × 0·75	67·5	
		outer rim	0·706117	9	0·5 × 3·5 × 0·5	63·8–65·0	
	pl 6–04	core (mi)	0·706305	11	0·55 × 0·4 × 0·75	66·0–83·5	
		outer core (mi)	0·706086	9	1 × 2 × 0·75	80·4–82·5	
		rim	0·706119	10	0·1 × 2·8 × 0·25	65·6–66·7	

B × L × D, breadth × length × depth (mm) of drilling; ol, olivine inclusions; mi, melt inclusions. The second number in the mineral name indicates the thick section number. As a result of the high error in the published Sr isotope composition of the STR45 whole-rock (Francalanci *et al.*, 1988), $^{87}Sr/^{86}Sr$ was re-analysed at the Dipartimento di Scienze della Terra of the University of Florence, using a Finnigan Triton TI, and standard chromatographic Sr separation technique.

analysis, were the same as those described by Longerich *et al.* (1996). Analysis of candidate glass reference materials BCR-2G, BHVO-1G and BIR-1G from the USGS gave results within 15% of the suggested reference values for all trace elements at concentrations >1 ppm and within 30% for trace elements <1 ppm.

Representative electron microprobe analyses, Sr isotope ratios and trace element analyses of all the analysed plagioclase and clinopyroxene are reported in Tables 1–4. The full mineral chemistry dataset is given in Electronic Appendices 1 and 2, which are available for downloading from http://www.petrology.oupjournals.org.

RESULTS

Petrographic studies have demonstrated that some microdrilled mineral cores contain melt inclusions. There appears to be no systematic difference, however, in Sr isotope composition between inclusion-bearing and inclusion-free samples (Table 1; Figs 5 and 6). This suggests isotopic equilibrium between melt inclusions and the host zone of the minerals. The drilled portion of some of the clinopyroxene cores also contains included olivine. Measured Sr isotope ratios are similar to those of other clinopyroxenes, suggesting that the $^{87}Sr/^{86}Sr$ of the olivines are the same as the coexisting clinopyroxenes, and/or that the low Sr abundances of olivine do not influence the measured $^{87}Sr/^{86}Sr$ (Table 1; Figs 5 and 6).

Two major observations can be made from the data presented in Table 1. First, from AD 1984 to 1996, there was a general decrease in Sr isotope ratios, not only among whole-rocks, but also among glassy groundmasses and phenocryst rims (Figs 5 and 6). Second, significant Sr isotope ratio variations are recorded in all the analysed minerals, and between minerals and their host groundmass. These data clearly establish that dynamic magmatic processes have caused recent and incomplete mixing of components within the magma plumbing system beneath Stromboli. This isotopic disequilibrium is more extensive in HP-magmas than LP-magmas (Table 1; Figs 5 and 6).

STR202 lava sample

Minerals from STR202 were the first to be microdrilled. Initial sampling involved larger areas than subsequent samples because of initial lack of confidence in the ability to transfer all the drilled material to cleaned Teflon beakers for Sr isotope analysis. Having demonstrated that the sample handling technique was efficient, subsequent minerals where sampled on a smaller scale. The net effect is that multiple growth zones were sampled from parts of STR202 minerals. It should be noted, however, that the two analysed plagioclases show similar

Table 2: Representative electron microprobe analyses of clinopyroxene

Sample:	STR45	STR45	STR45	STR45	STR45	STR45	STR45	STR45	STR45	STR9/96e	STR9/96e	STR9/96e	STR9/96e	STR9/96e	STR9/96e	STR9/96e	STR9/96d	STR9/96d	STR9/96d	STR9/96d
Grain:	cpx 1–92	cpx 1–92	cpx 1–92	cpx 1–92	cpx 1–92	cpx 1–92	cpx 1–92	cpx 1–92	cpx 1–92	cpx 1–03	cpx 2–03	cpx 2–03	cpx 2–03	cpx 2–03	cpx 2–03	cpx 2–03	cpx 1–02	cpx 1–02	cpx 1–02	cpx 1–02
Zone:	core	core	core	core	core	core	outer core	rim	outer rim	core	core	outer core	outer core	rim	rim	rim	core	core	core	rim
SiO_2	53·90	51·17	54·37	52·15	53·07	51·57	53·68	51·29	51·29	51·14	49·79	51·93	52·90	51·78	51·20	51·70	52·50	51·30	50·90	50·65
TiO_2	0·29	0·72	0·27	0·36	0·26	0·69	0·28	0·73	0·83	0·86	0·99	0·75	0·41	0·81	0·93	0·84	0·71	1·01	1·03	0·67
Al_2O_3	1·26	3·15	0·75	2·37	2·30	3·31	1·99	3·06	3·00	3·59	3·90	2·84	2·81	3·35	3·83	3·32	2·34	3·55	3·70	5·21
Cr_2O_3	0·04	0·09	0·05	0·43	0·62	0·09	0·50	0·08	0·04	0·03	0·01	0·04	0·23	0·01	0·03	0·03	0·03	0·04	0·01	0·14
FeO	4·78	7·34	6·09	6·95	3·35	6·42	3·39	7·49	8·29	9·91	10·13	8·10	6·35	8·28	8·91	8·70	8·67	8·51	9·00	5·18
MnO	0·13	0·20	0·25	0·19	0·10	0·17	0·10	0·19	0·20	0·28	0·30	0·22	0·15	0·23	0·23	0·25	0·26	0·25	0·24	0·13
MgO	17·01	15·06	18·14	15·40	16·77	15·21	17·05	14·80	14·56	14·21	13·35	14·84	15·41	14·32	14·01	14·14	14·65	13·93	13·82	14·81
CaO	22·36	21·73	19·73	21·80	23·08	22·23	23·01	21·79	21·63	20·16	20·22	21·66	21·92	21·58	21·30	21·52	21·16	21·85	21·42	23·06
Na_2O	0·18	0·33	0·24	0·32	0·19	0·32	0·16	0·33	0·32	0·36	0·42	0·31	0·24	0·32	0·40	0·35	0·34	0·34	0·37	0·19
Sum	99·98	99·84	99·93	99·97	99·74	100·04	100·19	99·76	100·17	100·59	99·16	100·73	100·43	100·69	100·90	100·86	100·66	100·77	100·53	100·07
Si	1·970	1·901	1·986	1·930	1·940	1·904	1·951	1·907	1·906	1·898	1·882	1·915	1·938	1·911	1·892	1·908	1·938	1·897	1·890	1·863
Ti	0·008	0·020	0·007	0·010	0·007	0·019	0·008	0·020	0·023	0·024	0·028	0·021	0·011	0·023	0·026	0·023	0·020	0·028	0·029	0·019
Al	0·054	0·138	0·032	0·103	0·099	0·144	0·085	0·134	0·131	0·157	0·174	0·123	0·121	0·146	0·167	0·144	0·102	0·155	0·162	0·226
Cr	0·001	0·003	0·002	0·013	0·018	0·003	0·014	0·002	0·001	0·001	0·000	0·001	0·007	0·000	0·001	0·001	0·001	0·001	0·000	0·004
Fe	0·146	0·228	0·186	0·215	0·102	0·198	0·103	0·233	0·258	0·308	0·320	0·250	0·195	0·255	0·275	0·269	0·268	0·263	0·280	0·159
Mn	0·004	0·006	0·008	0·006	0·003	0·005	0·003	0·006	0·006	0·009	0·010	0·007	0·004	0·007	0·007	0·008	0·008	0·008	0·008	0·004
Mg	0·927	0·834	0·988	0·850	0·914	0·837	0·924	0·821	0·806	0·786	0·752	0·816	0·841	0·787	0·772	0·778	0·806	0·768	0·765	0·812
Ca	0·876	0·865	0·772	0·864	0·904	0·880	0·896	0·868	0·861	0·802	0·819	0·856	0·860	0·853	0·843	0·851	0·837	0·866	0·852	0·909
Na	0·013	0·024	0·017	0·023	0·013	0·023	0·011	0·024	0·023	0·026	0·030	0·022	0·017	0·023	0·029	0·025	0·024	0·024	0·026	0·014
Cations	4·000	4·020	3·999	4·014	4·000	4·014	3·996	4·015	4·015	4·012	4·017	4·012	3·995	4·005	4·014	4·007	4·004	4·010	4·013	4·010
Charge	11·998	11·999	12·001	12·001	11·998	11·998	11·998	11·996	11·997	12·000	11·998	11·998	11·999	12·001	12·003	11·996	12·003	12·002	12·000	12·000
Mg-no.	0·86	0·79	0·84	0·80	0·90	0·81	0·90	0·78	0·76	0·72	0·70	0·77	0·81	0·76	0·74	0·74	0·75	0·74	0·73	0·84

Mg-no., molar $Mg^{2+}/(Mg^{2+} + Fe^{2+})$. The full mineral chemistry dataset is given in Electronic Appendix 1, which is available for downloading from http://www.petrology.oupjournals.org.

Table 3: Representative electron microprobe analyses of plagioclase

Sample:	STR45	STR45	STR45	STR45	STR45	STR45	STR9/96e	STR9/96e	STR9/96e	STR9/96e	STR9/96e	STR9/96e	STR9/96e	STR9/96e	STR9/96e	STR9/96e	STR9/96d	STR9/96d	STR9/96d	STR9/96d
Grain:	pl 6–91	pl 6–91	pl 6–91	pl 6–91	pl 6–91	pl 6–91	pl 4–03	pl 4–03	pl 4–03	pl 4–03	pl 4–03	pl 4–03	pl 4–03	pl 4–03	pl 4–03	pl 4–03	pl 3–02	pl 3–02	pl 3–02	pl 4–00
Zone:	core	core	outer core	rim	rim	outer core	core	core	core	core	outer core	outer core	rim	rim	rim	rim	core	core	core	rim
SiO_2	50·11	49·36	48·08	51·83	51·15	51·85	50·60	46·80	49·42	51·20	46·87	47·11	52·18	50·68	52·26	50·75	48·73	47·70	47·73	45·30
TiO_2	0·04	0·02	0·05	0·04	0·05	0·05	0·04	0·05	0·04	0·08	0·06	0·03	0·07	0·05	0·07	0·05	0·08	0·04	0·04	0·04
Al_2O_3	31·13	31·87	32·72	29·72	30·05	29·82	30·77	33·42	31·70	30·75	33·59	33·50	29·89	31·12	29·76	30·67	31·80	32·97	32·96	33·85
Fe_2O_3	0·88	0·87	0·85	0·76	0·94	0·91	0·93	0·87	0·86	0·93	0·90	0·92	0·81	0·90	0·83	0·92	1·10	0·70	0·74	0·66
MgO	0·10	0·09	0·09	0·10	0·12	0·12	0·13	0·08	0·12	0·14	0·09	0·07	0·12	0·11	0·12	0·12	0·47	0·19	0·16	0·12
CaO	14·29	15·15	16·27	13·12	13·26	12·94	14·19	17·09	15·06	13·95	17·36	17·13	13·12	14·31	12·96	14·03	16·08	16·79	17·06	17·71
SrO	0·18	0·15	0·17	0·15	0·18	0·31	0·19	0·16	0·19	0·15	0·20	0·20	0·19	0·19	0·23	0·24	0·18	0·20	0·21	0·10
Na_2O	2·87	2·59	2·05	3·65	3·47	3·60	3·00	1·49	2·49	3·11	1·43	1·66	3·55	3·03	3·66	3·07	2·05	1·83	1·73	1·25
K_2O	0·51	0·42	0·30	0·78	0·68	0·69	0·53	0·18	0·41	0·57	0·17	0·20	0·68	0·49	0·73	0·55	0·42	0·23	0·19	0·10
Sum	100·11	100·52	100·58	100·15	99·90	100·30	100·38	100·13	100·28	100·88	100·67	100·82	100·61	100·87	100·62	100·40	100·90	100·64	100·82	99·11
Si	2·291	2·252	2·199	2·363	2·340	2·361	2·307	2·154	2·259	2·320	2·148	2·155	2·366	2·299	2·370	2·313	2·223	2·182	2·181	2·110
Ti	0·001	0·001	0·002	0·001	0·002	0·002	0·001	0·002	0·001	0·003	0·002	0·001	0·002	0·002	0·003	0·002	0·003	0·001	0·001	0·001
Al	1·676	1·713	1·763	1·596	1·619	1·599	1·652	1·811	1·706	1·641	1·813	1·805	1·596	1·662	1·589	1·646	1·709	1·777	1·774	1·857
Fe	0·030	0·030	0·029	0·026	0·032	0·031	0·032	0·030	0·030	0·032	0·031	0·031	0·028	0·031	0·028	0·031	0·038	0·024	0·025	0·023
Mg	0·007	0·006	0·006	0·007	0·008	0·008	0·009	0·006	0·008	0·009	0·006	0·005	0·008	0·008	0·008	0·008	0·032	0·013	0·011	0·008
Ca	0·700	0·741	0·797	0·641	0·650	0·631	0·693	0·843	0·738	0·677	0·852	0·840	0·637	0·696	0·630	0·685	0·786	0·823	0·835	0·884
Sr	0·005	0·004	0·004	0·004	0·005	0·008	0·005	0·004	0·005	0·004	0·005	0·005	0·005	0·005	0·006	0·006	0·005	0·005	0·005	0·003
Na	0·255	0·229	0·182	0·323	0·308	0·318	0·265	0·133	0·221	0·274	0·127	0·148	0·312	0·267	0·322	0·271	0·181	0·162	0·153	0·113
K	0·030	0·025	0·018	0·045	0·040	0·040	0·031	0·010	0·024	0·033	0·010	0·012	0·039	0·028	0·042	0·032	0·025	0·013	0·011	0·006
Cations	4·995	5·001	5·000	5·006	5·004	4·998	4·995	4·993	4·992	4·993	4·994	5·002	4·993	4·998	4·998	4·994	5·002	5·000	4·996	5·005
Ab	25·9	23·0	18·3	32·0	30·9	32·2	26·8	13·5	22·5	27·8	12·8	14·8	31·6	26·9	32·4	27·4	18·2	16·2	15·3	11·3
An	71·1	74·5	79·9	63·5	65·1	63·8	70·1	85·5	75·1	68·8	86·1	84·0	64·5	70·2	63·4	69·3	79·2	82·5	83·6	88·1
Or	3·0	2·5	1·8	4·5	4·0	4·0	3·1	1·0	2·4	3·4	1·0	1·2	3·9	2·8	4·2	3·2	2·5	1·3	1·1	0·6

The full mineral chemistry dataset is given in Electronic Appendix 2, which is available for downloading from http://www.petrology.oupjournals.org

Table 4: Trace element composition (ppm) of clinopyroxene (cpx), plagioclase (pl) and melt inclusions (melt incl.) in STR45 and STR09/96e

Mineral:	cpx	cpx	cpx	cpx	melt incl.	melt incl.	cpx	cpx	cpx	cpx	cpx	cpx	cpx	cpx	pl	pl
Sample:	STR09/96e	STR09/96e	STR09/96e	STR45	STR45	STR45	STR45	STR45	STR45	STR45	STR45*	STR45	STR45	STR45*	STR45	STR45
Grain:	cpx 1–03	cpx 1–03	cpx 1–03	cpx 1–92	cpx 1–92	cpx 1–92	cpx 1–92	cpx 1–92	cpx 5–91	cpx 5–91	cpx 5–91	cpx 3–91	cpx 3–91	cpx 3–91	pl 6–91	pl 6–91
Zone:	core	inner rim	rim	core	melt incl.	melt incl.	outer core	outer rim	core	outer core	outer rim	core	inner rim	rim	inner rim	outer rim
Note:	Old	HP	HP	LP	in core LP	core(cpx+ol)	LP	HP	Old	LP ?	HP	HP	HP ?	HP	HP-LP mix	HP
$^{87}Sr/^{86}Sr$:	0·706331	0·706116	0·706124	0·706177	0·706177 ?	0·706335 ?	0·706154	0·706272	0·706325	0·706185	0·706285	0·706289	?	0·706283	0·706265	0·706289
Rb	—	—	—	1·73	21·8	58·0	—	0·32	—	0·48	8·93	—	—	13·4	6·76	4·08
Sr	77·3	70·8	61·4	76·3	135	132	64·0	67·1	61·2	68·7	91	63·1	83	124	1187	1469
Y	30·8	25·2	27·0	11·5	14·8	23·5	8·4	27·3	30·2	28·2	28·1	31·0	22·9	30·0	2·0	0·9
Zr	66·7	48·9	48·7	7·6	35·7	89·5	12·4	50·8	46·6	54·8	64·5	61·8	43·9	76·0	12·6	4·8
Nb	0·24	0·20	0·15	0·25	4·63	9·81	—	0·22	0·21	0·25	2·69	0·37	0·19	4·80	1·59	0·70
Ba	1·07	1·89	1·14	16·7	209	242	0·43	3·29	6·73	2·88	104	2·65	7·53	183	445	546
La	10·1	7·9	7·7	2·5	10·2	23·0	2·3	8·2	8·1	8·7	13·3	9·0	7·2	17·5	9·0	7·5
Ce	34·1	27·7	27·1	9·5	22·5	55·2	9·0	28·6	28·8	29·8	37·4	31·1	25·9	46·2	14·6	11·4
Pr	5·94	4·87	4·84	1·61	3·03	7·16	1·70	5·13	5·12	5·30	5·88	5·45	4·46	6·93	1·51	1·12
Nd	31·8	25·9	25·9	7·5	12·8	30·9	8·2	27·0	27·2	28·3	30·2	29·1	24·1	33·6	5·4	3·8
Sm	9·01	7·26	7·37	2·44	3·44	7·77	2·66	7·65	7·82	8·23	8·04	8·70	6·68	8·76	0·85	0·59
Eu	2·11	1·71	1·60	0·67	0·75	1·64	0·73	1·74	1·51	1·79	1·88	1·95	1·60	1·94	0·94	0·79
Gd	8·76	6·76	7·04	2·58	3·55	6·38	2·59	6·99	7·41	7·55	7·45	7·77	6·14	8·01	0·56	0·44
Tb	1·16	0·92	0·95	0·36	0·50	0·88	0·33	1·01	1·03	1·08	1·01	1·12	0·85	1·14	0·08	0·06
Dy	6·64	5·35	5·75	2·31	2·91	4·78	1·82	5·74	6·21	5·87	5·78	6·35	4·73	6·16	0·35	0·19
Ho	1·15	0·93	1·01	0·42	0·53	0·93	0·34	1·03	1·10	1·09	1·07	1·18	0·85	1·19	0·06	0·05
Er	2·89	2·37	2·48	1·21	1·50	2·31	0·83	2·54	2·94	2·71	2·64	2·93	2·27	2·74	0·17	0·08
Tm	0·39	0·32	0·33	0·19	0·21	0·30	0·10	0·35	0·38	0·32	0·37	0·40	0·30	0·40	0·03	0·02
Yb	2·52	1·99	2·21	1·15	1·58	1·86	0·67	2·19	2·56	2·36	2·33	2·68	1·82	2·47	0·17	0·09
Lu	0·37	0·28	0·30	0·19	0·25	0·28	0·09	0·33	0·37	0·35	0·32	0·39	0·28	0·40	0·03	0·04
Hf	2·68	1·94	2·07	0·30	0·74	2·49	0·61	2·07	1·76	2·30	2·29	2·54	1·80	2·43	0·28	0·09
Ta	0·05	0·03	0·03	—	0·33	0·56	—	0·04	0·03	0·03	0·18	0·08	0·03	0·32	0·09	0·06
Pb	0·30	0·31	0·37	0·46	4·11	9·13	0·21	0·34	0·41	0·46	2·31	0·42	0·32	3·70	9·51	5·24
Th	0·28	0·19	0·16	0·15	3·53	6·57	0·06	0·22	0·22	0·20	1·89	0·29	0·19	3·22	1·21	0·41
U	—	—	—	—	0·95	1·81	—	—	—	—	0·47	0·17	0·06	0·99	0·38	0·22

*, Clinopyroxene + glass mixture.
—, below detection limit; $^{87}Sr/^{86}Sr$ are those determined in the microdrilled portions of minerals; LP, crystallized in the magma with low phenocryst content; HP, crystallized in the highly porphyritic magma; Old, from cumulus reservoir.

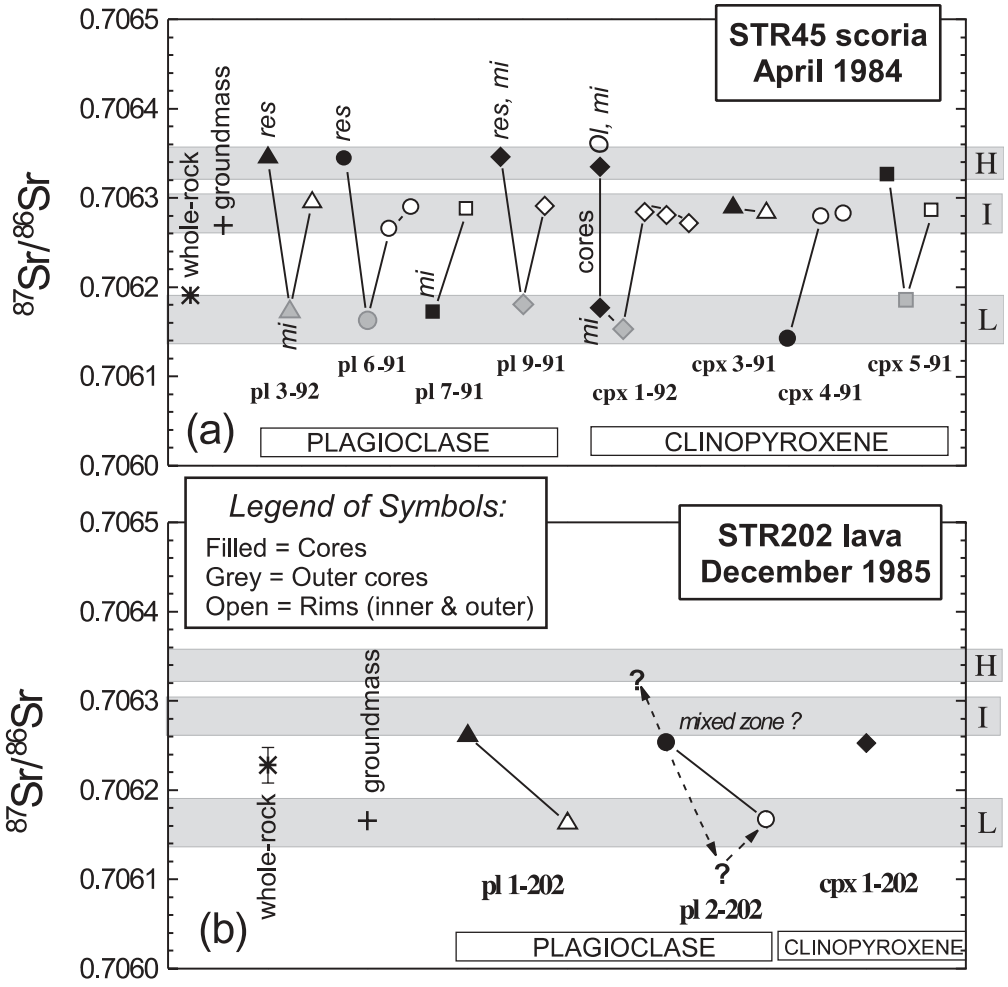

Fig. 5. Sr isotope data for samples (a) STR45 (scoria erupted during normal Strombolian activity on 28 April 1984); (b) STR202 (lava erupted in December 1985), measured in whole-rocks, glassy groundmasses and core–rim traverses of plagioclase and clinopyroxene. Each mineral is reported with a different symbol and the number of the mineral analysed (Table 1) is also shown. For each mineral, the range of variation is shown from core (filled symbol), to outer core (grey symbol), up to the outer rim (open symbol). Ol, olivine inclusion; mi, melt inclusions; res, resorbed; H, group with high $^{87}Sr/^{86}Sr$ ratios; I, group with intermediate $^{87}Sr/^{86}Sr$ ratios; L, group with low $^{87}Sr/^{86}Sr$ ratios. Because the $^{87}Sr/^{86}Sr$ ranges of H-, I- and L-groups for STR202 lava cannot be defined, those of STR45 scoria are reported in (b). Mineral cores of STR202 are probably mixtures between the highest and lowest Sr radiogenic zones (between H- and L-groups), with the latter having $^{87}Sr/^{86}Sr$ lower than the rim value. See text for additional explanation. With the exception of a whole-rock composition, the 2σ error corresponds to the symbol size.

core–rim variations in Sr isotope ratios (Table 1), with higher values in the cores than in the rims. A clinopyroxene core has $^{87}Sr/^{86}Sr$ similar to that of the plagioclase cores, whereas the glassy groundmass has $^{87}Sr/^{86}Sr$ comparable with the plagioclase rims. The $^{87}Sr/^{86}Sr$ of the whole-rock is intermediate between the cores and groundmass values (Table 1; Fig. 5b).

STR45 scoria sample

The glassy groundmass of scoria STR45 has a Sr isotope ratio (0·706269 ± 8) significantly higher than that of whole-rock (0·706191 ± 8). Plagioclase and clinopyroxene show comparable Sr isotope variations, which are often oscillatory (Fig. 5a). The $^{87}Sr/^{86}Sr$ of most of the analysed cores, especially the resorbed ones, are higher than 0·7063, in the range 0·70632–0·70635. Electron microprobe analyses reveal a large range of compositional variation in these cores (An% of plagioclase 59–75; Mg-number of clinopyroxene 0·72–0·90; Figs 3 and 7; Table 1). Some cores, however, have Sr isotope ratios lower than those of the whole-rock, with values in the range 0·70614–0·70618. Similar Sr isotope compositions are also found in the layers grown immediately around the more radiogenic cores (outer cores). Cores and outer cores with these relatively low Sr isotope ratios show generally high An contents in plagioclase (76–80%) and Mg-number in clinopyroxene (0·83–0·91) (Figs 3 and 7; Tables 1–3). The external layers (inner rims, rims and outer rims) have higher $^{87}Sr/^{86}Sr$ values,

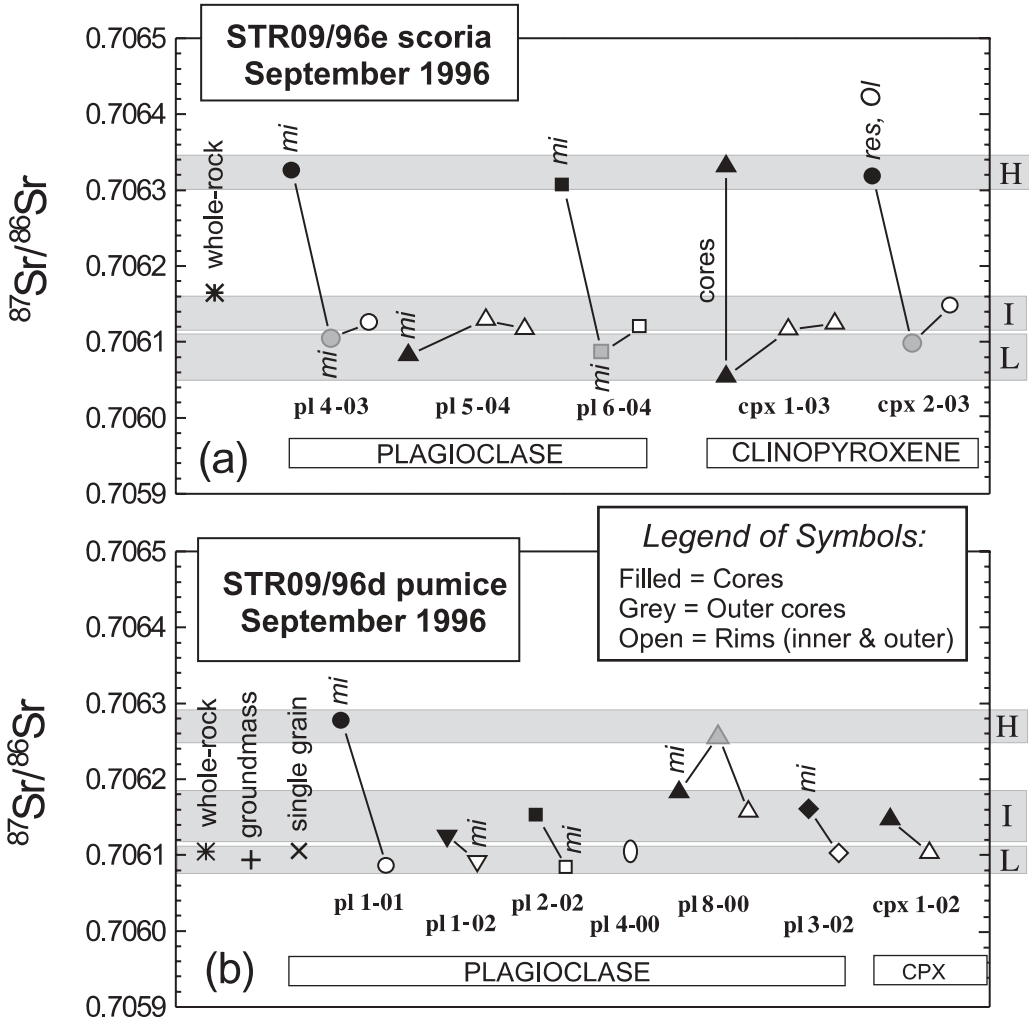

Fig. 6. Sr isotope data for coeval samples (a) STR09/96e (scoria) and (b) STR09/96d (pumice) erupted on 4 September 1996 from a major eruption. Values reported for whole-rocks, glassy groundmasses and core–rim traverses of plagioclase and clinopyroxene. Each mineral is reported with a different symbol and the number of the mineral analysed (Table 1) is also shown. For each mineral, the range of variation is shown from core (filled symbol), to outer core (grey symbol), up to outer rim (open symbol). CPX, clinopyroxene. 'Single grain' indicates the isotopic composition of a plagioclase microphenocryst which has been entirely drilled. Abbreviations as in Fig. 5. The $^{87}Sr/^{86}Sr$ ranges of H-, I- and L-groups refer to each sample. The 2σ error corresponds to the symbol size.

around 0·70628, that are comparable with those of the glassy groundmass and a clinopyroxene core (cpx 3–91, Fig. 5a). The latter core and all the external zones of plagioclase and clinopyroxene display lower An contents (58–66·5%) and Mg-number (0·74–0·78), respectively, than the growth zones with less radiogenic Sr (Figs 3 and 7; Tables 1–3).

Trace element contents have been determined in different zones of three clinopyroxenes and one plagioclase in sample STR45 (Table 4; Figs 8 and 9), together with two melt inclusions. Chondrite-normalized trace element contents of the clinopyroxenes are generally in the range from 0·1 to 40. For augitic zones (Mg-number <0·82), Rb_N, Ba_N, Nb_N and Pb_N are <1, Th_N, U_N, Ta_N and Sr_N are usually between 1 and 10, Hf_N, Zr_N, Y_N and heavy REE_N are around 10, and middle and light REE ($La–Dy_N$) are >10. Diopsidic (about Mg-number >0·82) zones have lower Hf_N, Zr_N, Y_N and REE_N (between 1 and 10, with $Ce–Gd_N$ around 10) (Fig. 8). The light REE have convex upwards patterns, which are less pronounced in the more diopsidic clinopyroxenes, whereas the heavy REE are fractionated with $Tb_N/Yb_N > 1$. All clinopyroxenes are characterized by small negative Eu anomalies (Eu/Eu* values between 0·68 and 0·75).

Two melt inclusions analysed in the core of cpx 1–92 have generally higher incompatible element contents (chondrite-normalized values are about 10 times those

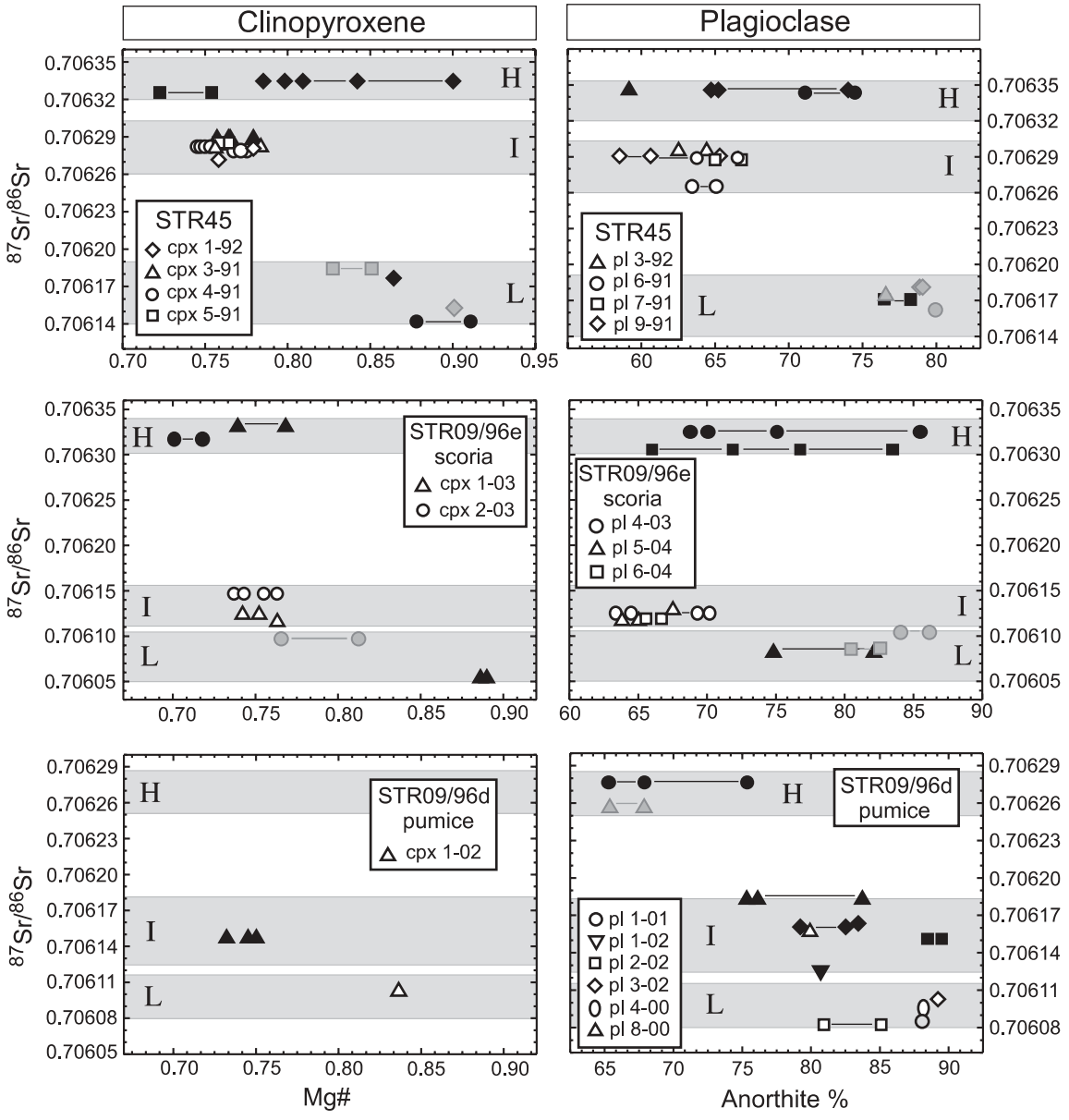

Fig. 7. Sr isotope composition versus Mg-number of clinopyroxene and An% of plagioclase for the analysed minerals. Each mineral is reported with a different symbol and the number of the mineral analysed (Table 1; Figs 5 and 6) is also shown. Filled symbols: cores; grey symbols: outer cores; open symbols: inner and outer rims. H, group with high $^{87}Sr/^{86}Sr$ ratios; I, group with intermediate $^{87}Sr/^{86}Sr$ ratios; L, group with low $^{87}Sr/^{86}Sr$ ratios. The $^{87}Sr/^{86}Sr$ ranges of H-, I- and L-groups refer to each sample and are not necessarily the same in all the rocks (see text for additional explanation). The 2σ error corresponds to the symbol size.

of the host clinopyroxene), with the exception of the heavy REE. REE patterns of melt inclusions are all fractionated with La_N/Sm_N and $Tb_N/Yb_N > 1$. Notably, the two melt inclusions are found in different portions of a single core: the inclusion less enriched in incompatible elements is present in the portion with low Sr isotope ratios, whereas the other inclusion is from the part of the core composed of clinopyroxene + olivine, which has a higher Sr isotope ratio (Fig. 8).

The outer rims of cpx 5–91 and cpx 3–91 have particularly high trace element contents and patterns with a similar shape to that of the melt inclusions. These analyses are interpreted as a mixture of clinopyroxene + glass, probably melt inclusions or interstitial matrix, which was not visible prior to the analyses (Fig. 8). Chondrite-normalized trace element contents of plagioclase are between 0·03 and 200 (Fig. 9). Heavy REE_N and, generally, Hf_N, Zr_N and Y_N are <1, light REE_N, Eu_N, Th_N and U_N are between 10 and 30, Ba_N and Sr_N

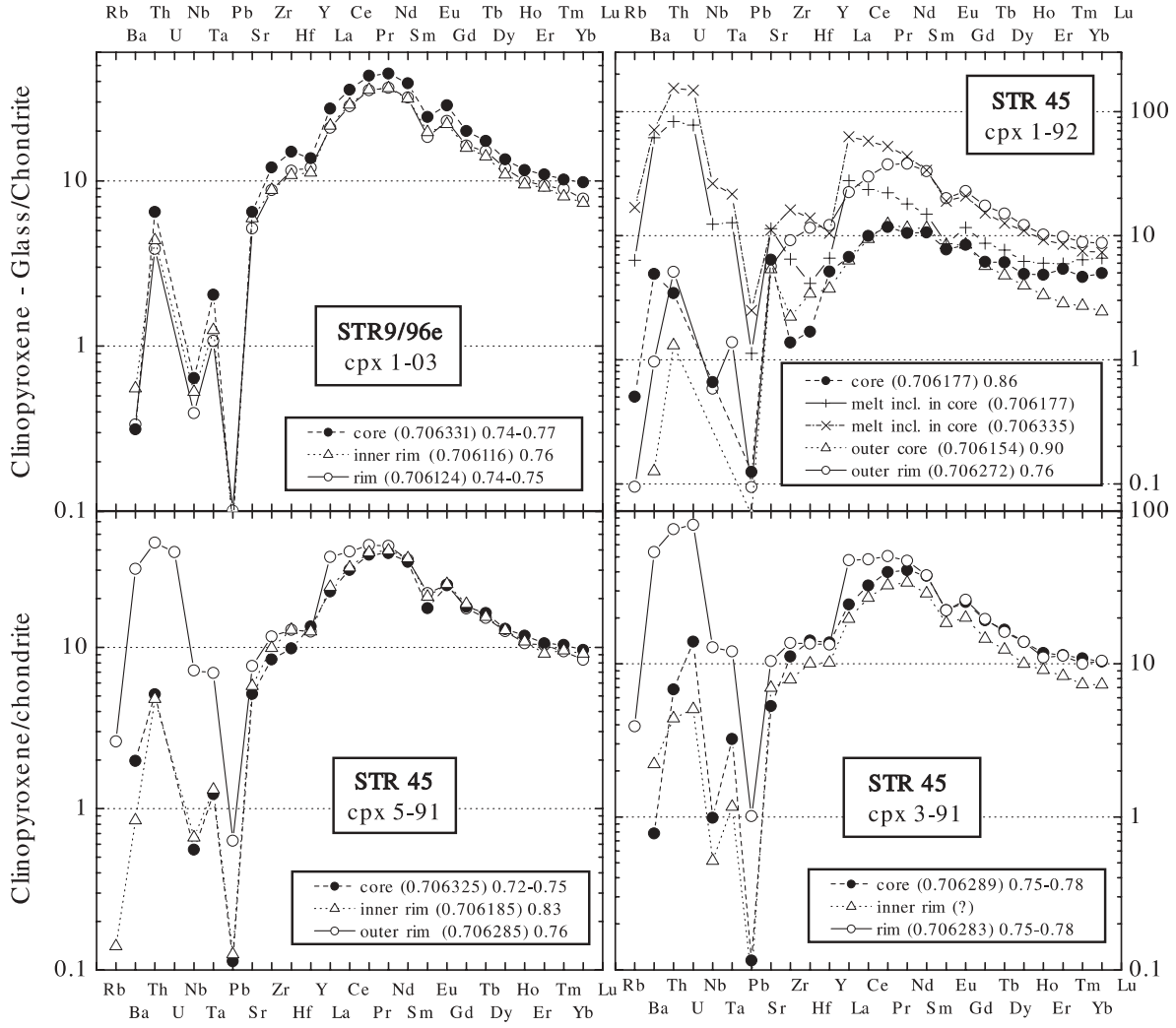

Fig. 8. Chondrite-normalized (Anders & Grevesse, 1989) trace element patterns for clinopyroxenes and melt inclusions of samples STR45 and STR09/96e. Element ordering: the REE have been divided from the other elements, which are in order of compatibility into a basaltic mineral assemblage. Sr isotope ratios and Mg-number of the analysed zones are also given in the legends. $^{87}Sr/^{86}Sr$ of melt inclusions refer to the isotopic composition of those zones in which mineral plus melt inclusions have been drilled.

are between 100 and 200. REE patterns are fractionated with $La_N/Yb_N > 1$ (Fig. 9).

STR09/96e scoria sample

Sr isotope ratio variations in plagioclase and clinopyroxene of scoria STR09/96e are mostly comparable, and range from 0·70606 to 0·70633. Cores, sometimes (about 50% of cores analysed) resorbed, are more radiogenic (0·70630–0·70633), whereas outer cores have lower $^{87}Sr/^{86}Sr$ values (0·70606–0·70610) (Fig. 6a; Table 1). The rims and outer rims record a minor increase in Sr isotope ratio, up to a maximum of 0·70615. One plagioclase crystal among those analysed has a less radiogenic core, with $^{87}Sr/^{86}Sr$ similar to those of the outer cores of the other crystals. The inner and outer rims of this plagioclase are isotopically comparable with the external layers of the other crystals analysed. Moreover, the core of cpx 1–03 has both the highest and lowest ratios found in this sample. The Sr isotope ratio of the whole-rock (0·706165 ± 8) is slightly higher than the rim values (Fig. 6a; Table 1). The more radiogenic cores show large major element variations, with An% of plagioclase cores between 65·5 and 85·5 and Mg-number of clinopyroxene cores between 0·70 and 0·77. The layers with less radiogenic Sr (cores and outer cores) usually have high An contents (75–86%) in plagioclase and high Mg-number (0·76–0·89) in clinopyroxene, whereas An contents (63–70·5%) and Mg-number (0·74–0·76) decrease towards the external layers (Figs 4 and 7; Tables 2 and 3).

Trace element contents have been determined in three zones of one clinopyroxene (cpx 1–03).

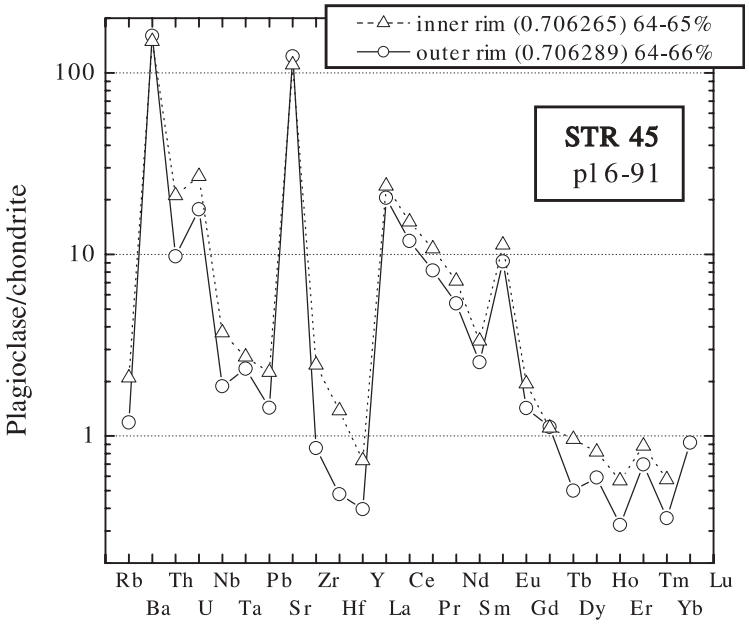

Fig. 9. Chondrite-normalized (Anders & Grevesse, 1989) trace element patterns for a plagioclase of sample STR45. See Fig. 8 for explanation of the element order. Sr isotope ratios and anorthite content (%) of the analysed zones are also given in the legend.

The chondrite-normalized patterns are similar to those of the augitic clinopyroxenes in the STR45 sample (Table 4; Fig. 8).

STR9/96d pumice sample

Different core–rim Sr isotope ratio variations are shown by the minerals of pumice STR9/96d. The whole-rock, the glassy groundmass, one single grain of plagioclase and all the rims of the minerals analysed have similar and relatively low $^{87}Sr/^{86}Sr$ values, close to 0·7061 (Fig. 6b; Table 1). About 80% of the analysed plagioclase cores and one clinopyroxene core have higher $^{87}Sr/^{86}Sr$, between 0·70613 and 0·70616. Two even higher Sr isotope ratios were found in a plagioclase core (0·70628) and in a plagioclase outer core (0·70626) (Fig. 6b). General negative correlations of Sr isotope ratios with the An content of plagioclase and Mg-number of clinopyroxene are observed. All the rims with low $^{87}Sr/^{86}Sr$ have $An_{81–90}$ and Mg-number of 0·84; the plagioclase cores and a rim with intermediate $^{87}Sr/^{86}Sr$ are between An_{75} and An_{84}, with only two data points at around An_{89} (Mg-number of clinopyroxene core is about 0·75), whereas the most radiogenic zones have $An_{65–75}$ (Fig. 7; Tables 2 and 3).

DISCUSSION

The dynamics of magmatic differentiation processes

A number of workers have proposed that the present-day plumbing system of Stromboli is close to steady-state conditions. This conclusion is based on thermal and gas budgets and the homogeneous composition of erupted rocks (Giberti *et al.*, 1992; Allard *et al.*, 1994, 2000; Harris & Stevenson, 1997; Francalanci *et al.*, 1999, 2004; Rosi *et al.*, 2000). A steady-state magma chamber system seems compatible with the presence of an open conduit system with nearly continuous eruptions. Accordingly, it has been suggested that the HP-magma, erupted mainly as black scoria and lavas, resides and evolves in a continuously erupting and crystallizing shallow reservoir that is replenished at a constant rate to maintain steady-state conditions (Francalanci *et al.*, 1999, 2004). In this model, the LP-magma, erupted as light pumice, represents the replenishing magma, which arrives from a deeper reservoir characterized by different physico-chemical conditions from that of the HP-magma reservoir (Francalanci *et al.*, 1999, 2004; Métrich *et al.*, 2001; Bertagnini *et al.*, 2003; Vaggelli *et al.*, 2003). Mixing associated with fractional crystallization is interpreted as the pre-eruptive process that controls the evolution of the magmas feeding the present-day activity of Stromboli.

Evidence of mixing between HP- and LP-magmas is provided by the oscillatory zoning of clinopyroxene and plagioclase (e.g. Figs 3 and 4) and the mixed nature of some scoria. Mixing has also been proposed based on melt inclusion data (Métrich *et al.*, 2001). Perhaps the most robust evidence of continuous mixing is the temporal decrease of Sr isotope ratios in scoria and lavas starting from AD 1980 (Fig. 2b). Francalanci *et al.* (1999) pointed out that the lowest Sr isotope ratios are recorded in the LP-magma pumice, which suggests that at about

1980, the shallow HP-magma reservoir started to be fed by magma with a different and lower Sr isotope signature. This replenishment led to the evolution of the shallow magmatic system towards a new isotopic equilibrium condition. The HP-magma has been interpreted as originally derived from an LP-magma with a higher Sr isotope ratio than that of the present-day LP-magma, by processes of plagioclase, clinopyroxene and olivine crystallization associated with periodic mixing with the feeding LP-magma (Francalanci *et al.*, 1999, 2004).

The results of this study have established that there is significant Sr isotope disequilibrium in clinopyroxene and plagioclase phenocrysts crystallized from magmas erupted during the present-day activity of Stromboli. There are systematic variations from core to rim recording the temporal evolution of the magma system. Despite concentrating the isotopic study on some of the most clearly zoned and generally larger phenocrysts, these results indicate that both plagioclase and clinopyroxene populations underwent similar temporal evolution during their crystallization history.

The different Sr isotope ratios recorded in all samples studied can be systematically divided into three groups, characterized by higher (H), lower (L) and intermediate (I) $^{87}Sr/^{86}Sr$ ratios. This does not mean, however, that these ratios are similar in the different samples, but the isotopic ratios are seen to decrease with the eruption age of the host magma. Furthermore, the mineral groups with the three isotope ratios have a different distribution in the scoria and pumice samples. In the scoria samples, comparable high $^{87}Sr/^{86}Sr$ values (H-group) are found in resorbed cores in both samples. Low $^{87}Sr/^{86}Sr$ values (L-group) are found in cores and/or outer cores, with the lowest values in the youngest samples. $^{87}Sr/^{86}Sr$ values intermediate between the H- and L-groups of the respective scoria (I-group) are usually found in rims, outer rims and the interstitial glass. These intermediate Sr isotope ratios also decrease from the older to the younger samples (Figs 5 and 6). L-group mineral growth zones always have higher An contents and Mg-numbers than I-group zones, whereas H-group cores show the largest ranges in major element composition (Fig. 7). In the pumice sample (STR9/96d), the highest $^{87}Sr/^{86}Sr$ ratios (H-group) are slightly lower than the H-group ratios of scoria samples. These compositions are again found in core and outer core regions of the phenocrysts. The lowest $^{87}Sr/^{86}Sr$ ratios (L-group) are found in rims and interstitial glass, and the $^{87}Sr/^{86}Sr$ ratios are comparable with the L-group ratios of the coeval scoria (STR9/96e). Intermediate $^{87}Sr/^{86}Sr$ ratios (I-group) are found in cores and an inner rim that are similar to the I-group ratios of the coeval scoria (Fig. 6b; Table 1). A general increase in An content and Mg-number is observed from H- to I- to L-group mineral zones in the pumice sample (Fig. 7).

Where Sr isotope ratios of interstitial glass were analysed, they were invariably very close to those of the respective crystal rims, suggesting isotopic equilibrium conditions between phenocryst rims and the glassy groundmass. Major element compositions were also used to establish equilibrium between phenocryst rims and microphenocrysts with their host glassy groundmasses (Francalanci *et al.*, 2004).

In both scoria samples, Sr isotope ratios increase towards the external zones of the plagioclase and clinopyroxene phenocrysts, starting from the lowest $^{87}Sr/^{86}Sr$ ratios (L-group) of cores and/or outer cores. In scoria STR09/96e, the L-group values (0·70605–0·70610) are comparable with the L-group values (0·70608–0·70610) registered in crystal rims, glass and whole-rocks of the coeval pumice STR09/96d (Fig. 6). This clearly indicates that the external zones of the plagioclase and clinopyroxene of both scoria samples crystallized concurrently with, or after, mixing between the LP- and HP-magmas. More specifically, these large and well zoned crystals seem to record a crystallization event in the LP-magma (registered by the L-group zones) followed by further crystallization during mixing with the HP-magma, which has a higher Sr isotope ratio (indicated by I-group zones).

These magmatic processes are also recorded by the major element compositions of the plagioclase and clinopyroxene growth zones. L-group mineral growth zones have compositions typical of equilibrium LP-magma minerals, and I-group mineral compositions zones are indistinguishable from equilibrium HP-magma minerals (Fig. 7).

In >50% of the analysed minerals in both scoria samples, the L-group zones occur immediately around cores (~50% resorbed) with the highest Sr isotope ratios (H-group). Combined L-group and H-group zones are also found to form some resorbed cores (Figs 5 and 6). The H-group $^{87}Sr/^{86}Sr$ values are higher than the whole-rock values and also higher than the $^{87}Sr/^{86}Sr$ values measured in the scoria and lavas of the 1906–1980 period (Fig. 2b). Magmas with higher Sr isotope ratios, however, have been erupted during the previous history of the volcano (Fig. 2a). The most recent example of high Sr isotope ratios is found in the San Bartolo lavas (younger than ~5 ka, but probably older than ~2 ka) (Figs 1 and 2a). Such a radiogenic Sr component has not previously been reported in the present-day magmas of Stromboli. The fact that this component is only found in crystal cores that are generally resorbed argues against the possibility that this isotopic signal records the presence of a third magma composition. Instead, it suggests the incorporation of previously accumulated mineral phases into the magma and the variable major element composition of the H-group zones strengthens this hypothesis (Fig. 7). These minerals are interpreted to have crystallized from older higher $^{87}Sr/^{86}Sr$ magmas. They

were later carried into the HP-magma chamber by the replenishing LP-magmas, as suggested by the L-group growth zones (formed in LP-magmas) around the H-group cores. The minerals are partially resorbed, probably during transportation, by the volatile-rich, hotter and more mafic LP-magmas. Later, as a consequence of cooling and degassing of the LP-magma at lower pressure, plagioclase and clinopyroxene nucleated upon the old resorbed grains in isotopic equilibrium with the LP-magma (L-group zones). Subsequent mixing of the LP-magma with the HP-magma in the shallow reservoir produced a new mixed magma with a higher Sr isotope ratio, from which the mineral rims crystallized with increased $^{87}Sr/^{86}Sr$ (I-group zones).

Some minerals of STR09/96e and STR45 scoria only have L-group cores (Figs 5 and 6), suggesting that these grains started to crystallize as nuclei in an LP-magma and not around old crystal nuclei remobilized from earlier cumulates. Likewise, the clinopyroxene core of STR45 scoria with a $^{87}Sr/^{86}Sr$ value similar to the rim values (cpx 3–91) is considered to be directly crystallized in the HP-magma. The available trace element data agree with the above interpretations. The two glass inclusions analysed in cpx 1–92 of STR45 constrain the composition of the melt in equilibrium with their different host clinopyroxenes (Table 3; Fig. 8). The melt inclusion with lower trace element contents is found in a diopsidic core, with L-group $^{87}Sr/^{86}Sr$ characteristics, that is considered to have crystallized from the less evolved LP-magma. In contrast, the melt inclusion more enriched in trace elements is present in a portion of a core with H-group $^{87}Sr/^{86}Sr$ characteristics, suggesting that the host clinopyroxene crystallized from a magma having higher incompatible element contents. The latter melt appears more fractionated, particularly given that most H-group clinopyroxenes and plagioclases show low Mg-number and An contents, respectively. Accordingly, even the H-group core of cpx 1–03 from the STR09/96e sample is slightly more enriched in trace elements than the I-group rims, even though they have a similar Mg-number (Fig. 8).

These results clearly demonstrate that the plumbing system of Stromboli contains a third component in addition to the HP- and LP-magmas. This component is represented by recycled plagioclase and clinopyroxene (and probably olivine) that form the resorbed cores of large phenocrysts. Evidence for mixing between the HP- and LP-magmas is clearly defined and indicates that this process occurs in a shallow magma chamber in which plagioclase crystallizes together with clinopyroxene (and olivine). Indeed, $^{87}Sr/^{86}Sr$ data for the external zones of both mineral phases rule out the possibility that this process takes place in the deeper LP-magma reservoir, where plagioclase crystallization does not occur (Francalanci *et al.*, 2004).

In the 1985 lava sample (STR202), the cores display similar $^{87}Sr/^{86}Sr$ values that are always higher than the rim values. H-group cores, however, are not tested in this sample (Fig. 5b). Minerals from this rock were sampled at the coarsest scale and the Sr isotope ratios of the cores are probably the result of mixing between more than one mineral zone. In contrast, the similarity of $^{87}Sr/^{86}Sr$ values of rims and groundmass seems to rule out the possibility that the plagioclase rims represent mixing of multiple crystal zones. Plagioclases from the 1985 lava always display oscillatory zoning with similar and quite low An contents in the rims (An contents = cores: 66–75%, intermediate bands: 75–83%, rims: 65–67%; De Fino *et al.*, 1988). This suggests that the rim $^{87}Sr/^{86}Sr$ composition of these feldspars does not represent that of the refilling LP-magma (L-group value), but records the Sr isotope ratio (I-group value) after mixing between the LP- and HP-magma (Fig. 5b). Accordingly, we conclude that, in December 1985, the $^{87}Sr/^{86}Sr$ value of the replenishing LP-magma was lower than the rim isotope value (0·70616).

The pumice STR09/96d is interpreted to represent the recharging LP-magma that is erupted during major eruptions, having had a minimal residence time in the shallow magma reservoir. Consequently, this LP-magma should record a different magmatic history from that of the LP-magma that remained in the shallow reservoir and completely mixed with the HP-magma. During eruption, pumices and scoria magmas are mingled at different scales, forming banded hand specimens and pumice in which the glass portions and minerals of the scoria are mingled on about a 100 μm scale (Francalanci *et al.*, 2004). In contrast, the pumice samples record no macroscopic evidence for mixing with the HP-magma. Consequently, rims of minerals and the glassy groundmass of the pumice, which have the least radiogenic measured $^{87}Sr/^{86}Sr$, are interpreted to represent the Sr isotope composition of the LP-magma. This hypothesis is supported by the fact that An contents and Mg-number of L-group rims are the highest recorded from recent magmas.

Most of the analysed crystal rims in the pumice, however, have grown around quite large cores (up to 2·5 mm) with I-group $^{87}Sr/^{86}Sr$ values (Figs 6b and 10a). The I-group $^{87}Sr/^{86}Sr$ values of the pumice STR09/96d (0·70612–0·70616) and the coeval scoria STR09/96e (0·70612–0·70615) are similar. I-group $^{87}Sr/^{86}Sr$ of the scoria are found in the crystal rims (Figs 6 and 7), and, consequently, represent the Sr isotope composition of minerals crystallized in equilibrium with the groundmass. These data suggest that the I-group cores within the LP-pumice may be xenocrysts deriving from the HP-magma during syn-eruptive mingling processes. The clinopyroxene compositions of I-group minerals are similar in all samples (Mg-number around 0·75 for STR09/96e and

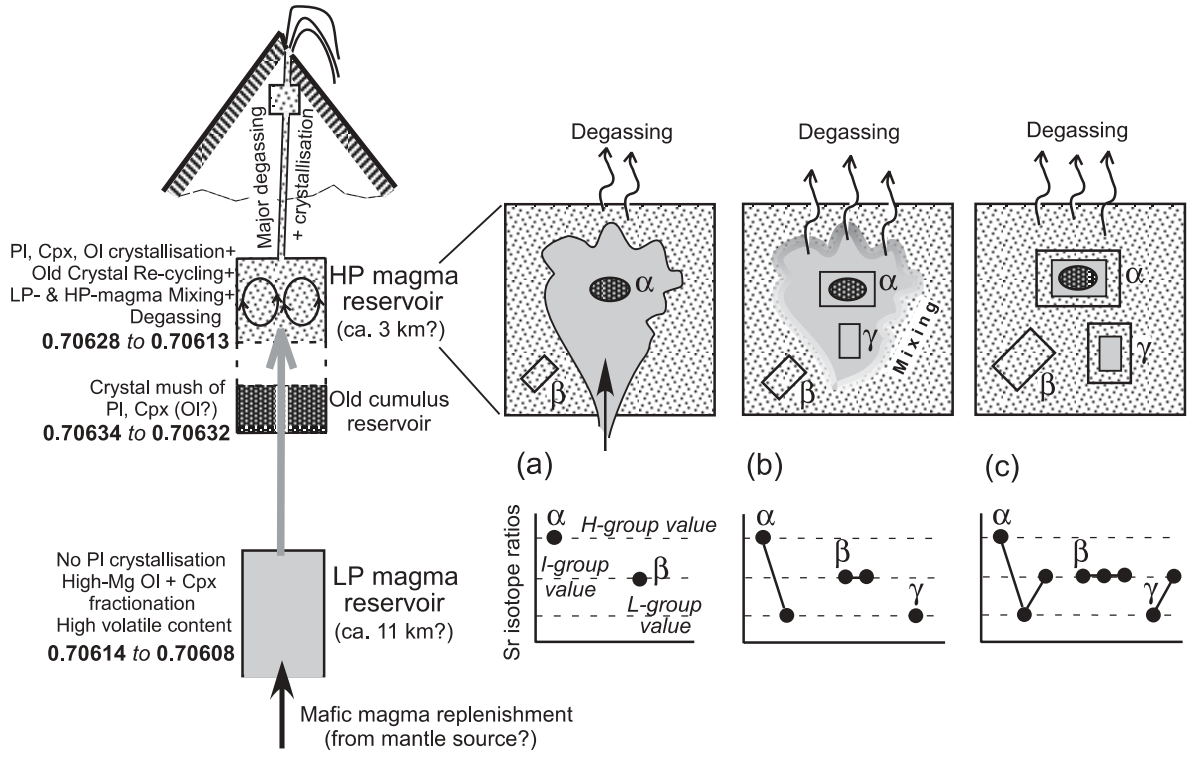

Fig. 10. Model of the sub-volcanic plumbing system and dynamics of Stromboli volcano. The two numbers in each magma reservoir are $^{87}Sr/^{86}Sr$ values, indicating the variation from AD 1984 to AD 1996. The H-, L-, I-group values and their core–rim distribution are referred to the three groups of Sr isotope ratios (highest, lowest and intermediate, respectively) that characterize the minerals of the scoria samples. Ol, olivine; Cpx, clinopyroxene; Pl, plagioclase. The reported depth values of HP- and LP-magmas derive from different calculations and considerations based on melt and fluid inclusion data in quartzite nodules entrained in calc-alkaline magmas (Vaggelli *et al.*, 2003) and olivine of LP-magmas (Bertagnini *et al.*, 2003). The small reservoir reported very close to the surface represents that directly feeding the normal Strombolian activity (Chouet *et al.*, 2003). α, β and γ are three representative minerals having different crystallization histories (e.g. pl 3–92, cpx 3–91 and pl 7–91 of STR45, respectively). (a), (b) and (c) (sketches and associated schematic diagrams) refer to three sequential time steps of a process cycle of crystallization plus mixing. For further explanation, see text.

STR09/96d; Fig. 7). I-group zone plagioclases in the LP-pumice, however, have higher An contents than the I-group zone plagioclases in the coeval scoria. This difference in plagioclase compositions suggests an important role for degassing processes in the Stromboli magmatic system. Water pressure has a far greater effect on plagioclase compositions than on pyroxene compositions, such that water loss from a rising volatile-saturated magma results in significantly less anorthitic plagioclase (McBirney, 1992). Thus, we argue that during its eruption and fast ascent to the surface, the LP-magma included plagioclase crystals that had crystallized from a magma isotopically similar to the HP-magma, but with a greater volatile content. This magma probably represents that residing in the shallow magma chamber, where it is subjected to mixing and fractional crystallization processes. Degassing during the relatively slow ascent of the HP-magmas through the conduit leads to re-equilibration of plagioclase compositions to the lower An contents (about 65%) typical of microphenocrysts and phenocryst rims of the HP-magmas. Considerations based on the different rheological characteristics of the HP- and LP-magmas have previously led to the suggestion that the two magmas mix easily when the HP-magma is not highly degassed (Francalanci *et al.*, 2004). H_2O exsolution associated with decompression mainly occurs during magma ascent through the conduit and causes additional magma crystallization (Métrich *et al.*, 2001).

The cumulus crystal mush reservoir

The presence of plagioclase and clinopyroxene cores with variable composition (Fig. 7) in isotopic disequilibrium with both LP- and HP-magmas has important implications for the plumbing system beneath Stromboli. These recycled minerals require the existence below the shallow reservoir feeding the present-day Strombolian activity of an older cumulus crystal mush zone, which is periodically disrupted and sampled by the ascending LP-magmas. The presence of plagioclase limits the depth of this mush zone to a shallow level. Examination of the Sr

isotope ratios of mineral cores can also help constrain the possible formation age of the mush zone. No magmas with Sr isotope ratios higher than 0·7063 have been erupted at Stromboli during the 20th century (Fig. 2b). The results of this paper have shown, however, that the whole-rock $^{87}Sr/^{86}Sr$ can be a mixture of core and rim components, thus, using whole-rock data might be misleading. Nevertheless, all the resorbed H-group cores have $^{87}Sr/^{86}Sr$ values between 0·70630 and 0·70635, and no cores record the value of about 0·70626, shown by scoria and lavas until AD 1980 (Fig. 2b). The fact that the latter Sr isotope ratio remained nearly constant for at least 80 years suggests a period during which the different processes combined to produce an isotopic steady-state. In this period, continuous mixing with an isotopically homogeneous LP-component could have masked the possible presence of mineral cores with H-group isotopic ratios. The lack of cores with $^{87}Sr/^{86}Sr$ around 0·70626 clearly indicates that cumulus crystals with this Sr isotopic composition were not formed recently. These considerations suggest that: (1) the cumulus crystal mush reservoir is older than AD 1900, (2) no crystals accumulated into the crystal mush from the HP-magmas during the last century, and (3) the shallow magma reservoir feeding the Strombolian activity is a homogeneous and well overturned reservoir that does not produce an extensive cumulate pile. Following this line of reasoning, it may be argued that the old crystal mush zone formed during a period characterized by less continuous activity, with reduced refilling and probable increased crystal fractionation. It has been suggested that such a style of activity occurred before the beginning of typical Strombolian activity (between the 3rd and 7th centuries AD) when there is little evidence of the frequent addition of LP-magma into a shallow magma reservoir (Rosi *et al.*, 2000).

Comparison with published whole-rock Sr isotope ratios suggests that the old crystal mush zone most probably represents the feeding reservoir of the San Bartolo lavas, erupted during the Recent period from an eccentric vent (Fig. 2a) (Francalanci *et al.*, 1988, 1989).

Temporal variations

A slight decrease in the H-group Sr isotope ratios seems to occur, passing from the scoria STR45 to STR09/96e (Figs 5 and 6). This may suggest a temporal decrease in $^{87}Sr/^{86}Sr$ in the crystal mush reservoir, probably because of the repeated transits of young, low $^{87}Sr/^{86}Sr$, LP-magmas. In addition, the $^{87}Sr/^{86}Sr$ values of L- and I-groups recorded by clinopyroxene and plagioclase decrease with time. The lowest recorded $^{87}Sr/^{86}Sr$ values of scoria STR09/96e are assumed to be representative of the Sr isotope composition of the LP-magma added to the magma chamber in 1996, as deduced by the similar L-group values of coeval scoria and pumice. If the same assumption is made for the scoria STR45, the $^{87}Sr/^{86}Sr$ of the LP-magma in April 1984 can be inferred from the L-group values. Between AD 1984 and 1996, the $^{87}Sr/^{86}Sr$ of the LP-magmas reduced from 0·70614 (the lowest value of L-group in STR45) to 0·70608 (the lowest value of L-group in pumice STR09/96d). As a result of the lack of dated pumice samples older than 1996, such a decrease was only previously inferred on the basis of Sr isotope variations in scoria and lavas (Francalanci *et al.*, 1999).

From April 1984 to September 1996, there is a significant decrease in Sr isotope ratios in the whole-rocks, the glassy groundmasses and the phenocryst rims. This change is particularly marked in the groundmasses and rims over about 1·5 years, from April 1984 to December 1985. Simple mixing calculations can be used to constrain the cause of this marked isotopic change. Ignoring the contribution of crystals, it is possible to calculate the amount of new LP-magma required to change the $^{87}Sr/^{86}Sr$ ratio of the 1985 lava groundmass. About 80% of the LP-magma groundmass with $^{87}Sr/^{86}Sr = 0{\cdot}70614$ (Sr = 700 ppm) needs to be mixed with 20% of STR45 scoria groundmass with $^{87}Sr/^{86}Sr = 0{\cdot}70628$ (Sr = 550 ppm) to produce the observed isotopic change. This conclusion disagrees with the minimal change in major and trace element contents of the HP-magmas over the same period of time. The input amount of the LP-magma, however, would be changed to <50% if a value of $^{87}Sr/^{86}Sr = 0{\cdot}70608$ was used for this magma. In the STR202 lava sample, a Sr isotope ratio of the LP-magma significantly lower than the rim/groundmass isotopic ratio (0·70616) has been proposed (see above). It is, therefore, deduced that the inferred temporal reduction in $^{87}Sr/^{86}Sr$ in the LP-magmas was not gradual, but occurred rapidly immediately before the eruption of the 1985 lava flows. It is, perhaps, significant that in the months prior to the 1985 lava eruption, the Strombolian activity was more intense, with very frequent and voluminous explosions. This observation implies the entry of an increased volume of LP-magma into the shallow magma chamber. The higher $^{87}Sr/^{86}Sr$ of the STR202 whole-rock compared with its groundmass, moreover, suggests that the increased volume of LP-magma entering the shallow magma reservoir also brought a large quantity of old cumulus mineral phases with H-group $^{87}Sr/^{86}Sr$ values.

Stromboli plumbing system and conclusions

The *in situ* geochemical and isotopic analyses presented here place important constraints on the present-day plumbing system of Stromboli (Fig. 10). The increase in Sr isotope ratios from outer cores towards the rims of plagioclase and clinopyroxene phenocrysts in scoria samples clearly defines a mixing process between

HP- and LP-magmas that occurs in a shallow magma chamber in which plagioclase crystallizes together with clinopyroxene (and olivine).

The most important contribution of this study has been the discovery of a third component in the plumbing system of Stromboli in addition to the HP- and LP-magmas. This component is represented by recycled minerals (at least plagioclase and clinopyroxene), found as the highly resorbed cores of large phenocrysts, derived from an older cumulus crystal mush zone, which is periodically disrupted and sampled by the ascending LP-magmas (Fig. 10).

Accordingly, the plumbing system of present-day Stromboli appears to be a polybaric multi-reservoir system, consisting of at least three different reservoirs. An additional reservoir is probably present at very shallow depths from which the Strombolian activity takes place (Chouet *et al.*, 2003) (Fig. 10). The LP-magma reservoir is situated at deeper level [probably at 10–11 km, according to Bertagnini *et al.* (2003) and Vaggelli *et al.* (2003), based on melt fluid inclusion data], and is periodically replenished by a mafic volatile-rich parental magma with relatively low Sr isotope ratios (L-group values ~0·70608). This reservoir is also characterized by fractional crystallization of mainly diopsidic clinopyroxene associated with minor forsteritic olivine. The LP-magma feeds the shallower reservoir containing the HP-magma [probably about 3 km deep, according to Vaggelli *et al.* (2003), based on melt fluid inclusion data]; the composition of the HP-magma appears to be derived from an LP-magma with more radiogenic Sr isotope ratios than the present-day LP-magma (0·70608), by a continuous process of plagioclase, clinopyroxene and olivine crystallization plus repeated mixing with the feeding LP-magma (Francalanci *et al.*, 1999, 2004). During the periodic magma recharge events, LP-magma passes through an old cumulus crystal mush reservoir. This mush reservoir must be situated just below the HP-magma chamber and contains plagioclase and clinopyroxene (and olivine?), with relatively high Sr isotope ratios (H-group value, >0·7063). These minerals are sampled by the LP-magma and transported into the shallower reservoir that is characterized by intermediate $^{87}Sr/^{86}Sr$ (I-group). The implications are that when the minerals from the mush reservoir enter the volatile-rich, hotter and more mafic LP-magmas, they are partially resorbed (crystal α of Fig. 10a). Following cooling and degassing at lower pressure, plagioclase and clinopyroxene re-crystallize around the old cores in isotopic equilibrium with the LP-magma (Fig. 10b). Contemporaneously, some new crystals nucleate and grow in the LP-magma (e.g. crystal γ of Fig. 10b). The physico-chemical changes to the LP-magma caused by degassing and crystallization in the shallow reservoir favour mixing with the HP-magma, generating a hybrid magma with intermediate Sr isotope ratios from which crystal rims with increased $^{87}Sr/^{86}Sr$ grow (rims of crystals α and γ of Fig. 10c). The high phenocryst content of the HP-magmas is also a result of mineral phases nucleating and growing directly in these magmas (crystal β of Fig. 10a–c). Several considerations, mainly based on the temporal evolution of Sr isotope compositions in the Recent period, lead us to hypothesize that the old cumulus reservoir is older than AD 1900, and that it probably formed in a period of reduced magma recharge and increased crystal fractionation.

The plagioclase cores with intermediate $^{87}Sr/^{86}Sr$ values (I-group) in the LP-magma STR09/96d are probably derived from the HP-magma by mingling processes. They are probably incorporated into the LP-magma when the two magmas first interact in the shallow reservoir. These plagioclases have high An contents (Fig. 7), suggesting that the HP-magma was not strongly degassed during interaction with the LP-magma. Relatively efficient mixing between the two magmas was therefore possible in the shallow reservoir because of their similar rheological characteristics. Further degassing of the HP-magma occurs as it moves along the conduit to the surface, during the relatively slow ascent associated with normal Strombolian activity. This leads plagioclase rims to form with the lower An contents typical of the plagioclase rim composition of scoria and lavas.

These data also provide evidence that the $^{87}Sr/^{86}Sr$ decrease in scoria and lavas starting from about AD 1980 is effectively because of the $^{87}Sr/^{86}Sr$ decrease of the LP-magma type—a variation that was only previously inferred from the Sr isotope variation of scoria and lavas (Francalanci *et al.*, 1999). The $^{87}Sr/^{86}Sr$ decrease of the LP-magma was probably very rapid, and occurred before the eruption of the 1985 lava flows. This temporal change seems to have been associated with an increased volume of LP-magma entering the shallow magma chamber, which caused the more intense Strombolian activity before the 1985 lava eruption.

ACKNOWLEDGEMENTS

The authors wish to thank John Wolff and two anonymous referees for thoughtful reviews and useful suggestions that greatly improved the paper. Marjorie Wilson's editorial input was, as always, extremely helpful. Financial support was provided by Italian Ministry of Protection through the 'Gruppo Nazionale di Vulcanologia', by the Università degli Studi di Firenze (ex 60% funds), and by Italian MIUR (FIRB_2001 and PRIN_2004 grants). Funding for the isotope and microprobe facilities at the VU was provided by NWO and the Vrije Universiteit. This is NSG publication 20050203.

SUPPLEMENTARY DATA

Supplementary Data for this paper are available at *Journal of Petrology* online.

REFERENCES

Allard, P., Carbonnelle, J., Métrich, N., Loyer, H. & Zettwoog, P. (1994). Sulphur output and magma degassing budget of Stromboli volcano. *Nature* **368**, 326–330.

Allard, P., Aiuppa, A., Loyer, H., Carrot, F., Gaudry, A., Pinte, G., Michel, A. & Dongarrà, G. (2000). Acid gas and metal emission rates during long-lived basalt degassing at Stromboli volcano. *Geophysical Research Letters* **27**, 1207–1210.

Anders, E. & Grevesse, N. (1989). Abundances of the elements: meteoric and solar. *Geochimica et Cosmochimica Acta* **53**, 197–214.

Barberi, F., Rosi, M. & Sodi, A. (1993). Volcanic hazard assessment at Stromboli based on review of historical data. *Acta Vulcanologica* **3**, 173–187.

Bertagnini, A., Coltelli, M., Landi, P., Pompilio, M. & Rosi, M. (1999). Violent explosions yield new insights into dynamics of Stromboli volcano. *EOS Transactions, American Geophysical Union* **80**, 635–636.

Bertagnini, A., Métrich, N., Landi, P. & Rosi, M. (2003). Stromboli volcano (Aeolian Archipelago, Italy): an open window on the deep-feeding system of a steady state basaltic volcano. *Journal of Geophysical Research* **108**(B7), 2336, doi: 10.1029/2002JB002146.

Bonaccorso, A., Cardaci, C., Coltelli, M., Del Carlo, P., Falsaperla, S., Panucci, S., Pompilio, M. & Villari, L. (1996). Annual report of the world volcanic eruptions in 1993, Stromboli. *Bulletin of Volcanic Eruptions* **33**, 7–13.

Bonaccorso, A., Calvari, S., Garfi, G., Lodato, L. & Patanè, D. (2003). Dynamics of the December 2002 flank failure and tsunami at Stromboli volcano inferred by volcanological and geophysical observations. *Geophysical Research Letters* **30**(18), 1941, doi: 10.1029/2003GLO17702.

Capaldi, G., Guerra, I., Lo Bascio, A., Luongo, G., Pece, R., Rapolla, A., Scarpa, R., Del Pezzo, E., Martini, M., Ghiara, M. R., Lirer, L., Munno, R. & La Volpe, L. (1978). Stromboli and its 1975 eruption. *Bulletin of Volcanology* **41**, 259–285.

Chouet, B., Dawson, P., Ohminato, T., Martini, M., Saccorotti, G., Giudicepietro, F., De Luca, G., Milana, G. & Scarpa, R. (2003). Source mechanisms of explosions at Stromboli Volcano, Italy, determined from moment tensor inversions of very-long-period data. *Journal of Geophysical Research* **108**(B1), 2109, doi: 10.1029/2002ID001919.

Davidson, J. P. & Tepley, F. J., III. (1997). Recharge in volcanic systems: evidence from isotope profiles of phenocrysts. *Science* **275**, 826–829.

Davidson, J. P., Tepley, F. J., III. & Knesel, K. M. (1998). Isotopic fingerprinting may provide insight into evolution of magmatic system. *EOS Transactions, American Geophysical Union* **79**, 185, 189, 193.

Davidson, J. P., Tepley, F. J., III, Palacs, Z. & Meffan-Main, S. (2001). Magma recharge, contamination and residence times revealed by *in situ* laser ablation isotopic analysis of feldspar in volcanic rocks. *Earth and Planetary Science Letters* **184**, 427–442.

De Fino, M., La Volpe, L., Falsaperla, S., Frazzetta, G., Neri, G., Francalanci, L., Rosi, M. & Sbrana, A. (1988). The Stromboli eruption of December 6, 1985–April 25, 1986: volcanological, petrological and seismological data. *Rendiconti della Società Italiana di Mineralogia e Petrologia* **43**, 1021–1038.

Feldstein, S. N., Halliday, A. N., Davies, G. R. & Hall, C. M. (1994). Isotope and chemical microsampling: constraints on the history of an S-type rhyolite, San Vincenzo, Tuscany, Italy. *Geochimica et Cosmochimica Acta* **58**, 943–958.

Francalanci, L., Barbieri, M., Manetti, P., Peccerillo, A. & Tolomeo, L. (1988). Sr-isotopic systematics in volcanic rocks from the island of Stromboli (Aeolian arc). *Chemical Geology* **73**, 164–180.

Francalanci, L., Manetti, P. & Peccerillo, A. (1989). Volcanological and magmatological evolution of Stromboli volcano (Aeolian islands): the roles of fractional crystallisation, magma mixing, crustal contamination and source heterogeneity. *Bulletin of Volcanology* **51**, 355–378.

Francalanci, L., Manetti, P., Peccerillo, A. & Keller, J. (1993). Magmatological evolution of the Stromboli volcano (Aeolian Arc, Italy): inferences from major and trace element and Sr-isotopic composition of lavas and pyroclastic rocks. *Acta Vulcanologica* **3**, 127–151.

Francalanci, L., Tommasini, S., Conticelli, S. & Davies, G. R. (1999). Sr isotope evidence for short magma residence time for the 20th century activity at Stromboli volcano, Italy. *Earth and Planetary Science Letters* **167**, 61–69.

Francalanci, L., Tommasini, S. & Conticelli, S. (2004). The volcanic activity of Stromboli in the 1906–1998 A.D. period: mineralogical, geochemical and isotope data relevant to the understanding of Strombolian activity. *Journal of Volcanology and Geothermal Research* **131**, 179–211.

Giberti, G., Jaupart, C. & Sartoris, G. (1992). Steady-state operation of Stromboli volcano, Italy: constraints on the feeding system. *Bulletin of Volcanology* **54**, 535–541.

Gillot, P. Y. & Keller, J. (1993). Radiochronological dating of Stromboli. *Acta Vulcanologica* **3**, 69–77.

Harris, A. J. L. & Stevenson, D. S. (1997). Magma budgets and steady state activity of Vulcano and Stromboli. *Geophysical Research Letters* **24**, 1043–1046.

Hornig-Kjarsgaard, I., Keller, J., Koberski, U., Stadlbauer, E., Francalanci, L. & Lenhart, R. (1993). Geology, stratigraphy and volcanological evolution of the island of Stromboli, Aeolian arc, Italy. *Acta Vulcanologica* **3**, 21–68.

Keller, J., Hornig-Kjarsgaard, I., Koberski, U., Stadlbauer, E. & Lenhart, R. (1993). Geological map of the island of Stromboli—scale 1:10 000. *Acta Vulcanologica* **3**, appendix.

Knesel, K. M., Davidson, J. P. & Duffield, W. A. (1999). Evolution of silicic magma through assimilation and subsequent recharge: evidence from Sr isotopes in sanidine phenocrysts, Taylor Creek Rhyolite, NM. *Journal of Petrology* **40**, 773–786.

Kokelaar, P. & Romagnoli, C. (1995). Sector collapse, sedimentation and clast population evolution at an active island-arc volcano: Stromboli, Italy. *Bulletin of Volcanology* **57**, 240–262.

Le Maitre, R. W. (2002). *A Classification of Igneous Rocks and Glossary of Terms*, 2nd edition. Cambridge: Cambridge University Press.

Longerich, H. P., Jackson, S. E. & Gunther, D. (1996). Laser ablation inductively coupled plasma mass spectrometric transient signal data acquisition and analyte concentration calculation. *Journal of Analytical Atomic Spectrometry* **11**, 899–904.

Luais, B. (1988). Mantle mixing and crustal contamination as the origin of the high-Sr radiogenic magmatism of Stromboli (Aeolian arc). *Earth and Planetary Science Letters* **88**, 93–106.

Mason, P. R. D. & Kraan, W. J. (2002). Attenuation of spectral interferences during laser ablation inductively coupled plasma mass spectrometry (LA–ICP–MS) using an rf only collision and reaction cell. *Journal of Analytical Atomic Spectrometry* **17**, 858–867.

McBirney, A. R. (1992). *Igneous Petrology*, 2nd edition. London: Jones and Bartlett, 508 pp.

Métrich, N., Bertagnini, A., Landi, P. & Rosi, M. (2001). Crystallization driven by decompression and water loss at Stromboli volcano (Aeolian Islands, Italy). *Journal of Petrology* **42**, 1471–1490.

Morelli, C., Giese, P., Cassinis, R., Colombi, B., Guerra, I., Luongo, G., Scarascia, S. & Shutte, K. G. (1975). Crustal structure of Southern Italy: a seismic refraction profile between Puglia–Calabria–Sicily. *Bollettino di Geofisica Teoricaed Applicata* **18**, 183–210.

Pasquarè, G., Francalanci, L., Garduño, V. H. & Tibaldi, A. (1993). Structure and geologic evolution of the Stromboli volcano, Aeolian islands, Italy. *Acta Vulcanologica* **3**, 79–89.

Pearce, N. J. G., Perkins, W. T., Wesgate, J. A., Gorton, M. P., Jackson, S. E., Neal, C. R. & Chenery, S. P. (1997). A compilation of new and published major and trace element data for NIST SRM 610 and NIST SRM 612 glass reference materials. *Geostandards Newsletter* **21**, 115–144.

Peccerillo, A. & Taylor, S. R. (1976). Geochemistry of Eocene calc-alkaline volcanic rocks from Kastamonu area, Northern Turkey. *Contributions to Mineralogy and Petrology* **58**, 63–81.

Perini, G., Tepley, F. J., III, Davidson, J. P. & Conticelli, S. (2003). The origin of K-feldspar megacrysts hosted in alkaline potassic rocks from central Italy: a track for low-pressure processes in mafic magmas. *Lithos* **66**, 223–240.

Ramos, F. C., Wolff, J. A. & Tollstrup, D. L. (2004). Measuring $^{87}Sr/^{86}Sr$ variations in minerals and groundmass from basalts using LA–MC–ICPMS. *Chemical Geology* **211**, 135–158.

Rosi, M. (1980). The Island of Stromboli. *Rendiconti della Società Italiana di Mineralogia e Petrologia* **36**, 345–368.

Rosi, M., Bertagnini, A. & Landi, P. (2000). Onset of the persistent activity at Stromboli volcano (Italy). *Bulletin of Volcanology* **62**, 294–300.

Singer, B. S., Dungan, M. A. & Layne, G. D. (1995). Textures and Sr, Ba, Mg, Fe, K, and Ti compositional profiles in volcanic plagioclase: clues to the dynamics of calc-alkaline magma chambers. *American Mineralogist* **80**, 776–798.

Tepley, F. J., III, Davidson, J. P. & Clynne, M. A. (1999). Magmatic interactions as recorded in plagioclase phenocrysts of Chaos Crags, Lassen Volcanic Center, California. *Journal of Petrology*, **40**, 787–806.

Tepley, F. J., III, Davidson, J. P., Tilling, R. I. & Arth, J. G. (2000). Magma mixing, recharge and eruption histories recorded in plagioclase phenocrysts from El Chichòn Volcano, Mexico. *Journal of Petrology* **41**, 1397–1411.

Tibaldi, A. (2001). Multiple sector collapses at Stromboli volcano: how they work. *Bulletin of Volcanology* **63**, 112–125.

Tibaldi, A., Corazzato, C., Apuani, T. & Cancelli, A. (2003). Deformation at Stromboli volcano (Italy) revealed by rock mechanics and structural geology. *Tectonophysics* **361**, 187–204.

Vaggelli, G., Francalanci, L., Ruggieri, G. & Testi, S. (2003). Persistent polybaric rests of calc-alkaline magmas at Stromboli volcano, Italy: pressure data from fluid inclusions in restitic quartzite nodules. *Bulletin of Volcanology* **65**, 385–404.

Wolff, J. A., Ramos, F. C. & Davidson, J. P. (1999). Sr isotope disequilibrium during differentiation of the Bandelier Tuff: constraints on the crystallisation of a large rhyolitic magma chamber. *Geology* **27**, 495–498.